Chinese Journal of Chemical Engineering 27 (2019) 1257–1271

Contents lists available at ScienceDirect

Chinese Journal of Chemical Engineering

journal homepage: www.elsevier.com/locate/CJChE

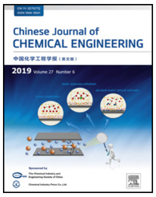

Review

Beyond graphene oxides: Emerging 2D molecular sieve membranes for efficient separation☆

Yi Liu

State Key Laboratory of Fine Chemicals, Dalian University of Technology, Linggong Road 2, Ganjingzi District, Dalian 116024, China

ARTICLE INFO

Article history:
Received 3 July 2018
Received in revised form 25 July 2018
Accepted 28 August 2018
Available online 6 September 2018

Keywords:
Two-dimentional material
Molecular sieves
Membranes
Separation
Desalination

ABSTRACT

Recent decades witnessed the significant progress made in the research field of 2D molecular sieve membranes. In comparison with their 3D counterparts, 2D molecular sieve membranes possessed several unique advantages like significantly reduced membrane thickness (one atom thick in theory) and diversified molecular sieving mechanisms (in-plane pores within nanosheets & interlayer galleries between nanosheets). M. Tsapatsis first carried out pioneering work on fabrication of lamellar ZSM-5 membrane. Since then, diverse 2D materials typically including graphene oxides (GOs) have been fabricated into membranes showing promising prospects in energy-efficient gas separation, pervaporation, desalination and nanofiltration. In addition to GOs, other emerging 2D materials, including 2D zeolites, 2D metal–organic frameworks (MOFs), 2D covalent-organic frameworks (COFs), layered double hydroxides (LDHs), transition metal dichalcogenides (TMDCs), MXenes (typically $Ti_3C_2T_X$), graphitic carbon nitrides (typically g-C_3N_4), hexagonal boron nitride (h-BN) and montmorillonites (MT) are showing intriguing performance in membrane-based separation process. This article summarized the most recent developments in the field of 2D molecular sieve membranes aside from GOs with particular emphasis on their structure–performance relationship and application prospects in industrial separation.

1. Introduction

As one of the most energy-consuming process, separation process accounts for 45%–55% of total energy consumption of the global industry [1]. It has therefore become increasingly urgent to develop energy-efficient separation processes to lift the heavy energy burdens. Membrane-based separation represented a relatively new concept but developed quickly due to the low energy consumption, high efficiency, sustainability and easy operation [2]. As an important sub-branch of membrane materials, molecular sieve-based membranes, which could achieve precise separation of multi-components relying on size-based exclusion and preferential adsorption mechanisms, have received tremendous attention in recent decades due to their permanent porosity, framework robustness and versatile available framework structures.

Conventional molecular sieve membranes contain three-dimensional (3D) framework topologies. Since the pioneering work on lamellar ZSM-5 membranes conducted by M. Tsapatsis [3], construction of high performance molecular sieve membranes from atom-thick two-dimensional (2D) nanosheets has become a frontier research topic. In comparison with their 3D counterparts, molecular sieve membranes constructed from 2D nanosheets could be only one-atom thick, therefore enabling minimization of the transport resistance and maximization of the flux; moreover, they were more mechanically flexible [4,5]. Particularly it should be emphasized that guest species enabled to permeate through 2D molecular sieve membranes and realize precise molecular sieving relying on either pores within 2D nanosheets (if any) or interlayer passages between neighboring nanosheets, which provides us with unprecedented freedom for tailoring their pore aperture and functionality (schematically shown in Fig. 1) [6,7]. All these advantages have made 2D molecular sieve membranes superb candidates of high-performance separation membranes.

Graphene and its derivatives are among the most extensively studied 2D layered materials [8]. Ever since the year 2012, great attention has been paid to graphene-based separation membranes [9,10] and several excellent review articles dealing with this topic have been published recently [11,12]. Aside from graphene and its derivatives, other emerging 2D layered materials typically including 2D zeolites, 2D MOFs, 2D COFs, LDHs, TMDCs, MXenes, g-C_3N_4, h-BN and MT have been fabricated into membranes with controlled microstructures and shown unprecedented opportunities in microfiltration, nanofiltration, ultrafiltration, reverse osmosis, pervaporation and gas separation [6,7,13–18]. Among them, guest molecules selectively permeated through 2D GO-, LDH-, TMDC-, MXene-, g-C_3N_4, h-BN and MT membranes *via* interlayer galleries, while in-plane pore-based molecular sieving represented the dominant separation mechanism for 2D zeolite-, 2D MOF- and COF-based membranes.

☆ Supported by the National Natural Science Foundation of China (21176231), the Fundamental Research Funds for the Central Universities (DUT16RC(3)103), and Thousand Youth Talents Program.

E-mail address: diligenliu@dlut.edu.cn.

https://doi.org/10.1016/j.cjche.2018.08.019
1004-9541/

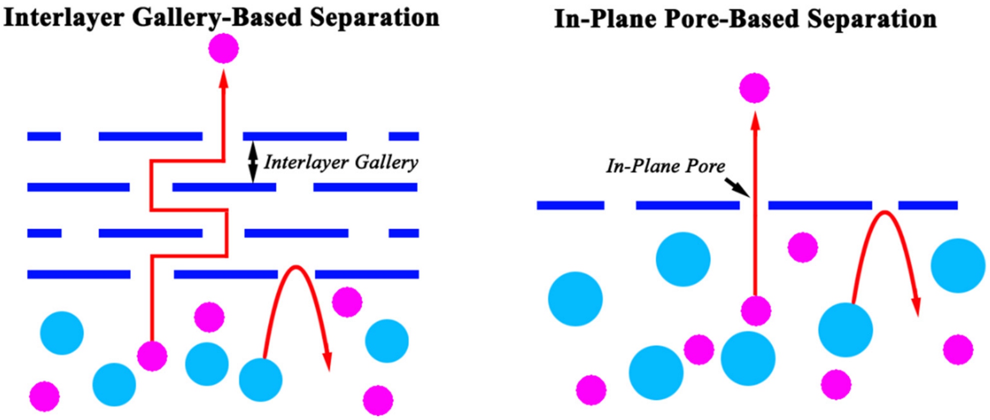

Fig. 1. Schematic illustration of both interlayer gallery-based and in-plane pore-based separation mechanisms for 2D separation membranes.

In this review article, the most recent developments in the field of 2D molecular sieve membranes are summarized with particular concerns over innovative methods, approaches and strategies developed for exerting precise control over their microstructures and functionality at microscopic, mesoscopic and macroscopic scales.

2. 2D materials employed in membrane-based separation

2.1. 2D zeolite membrane

By analogy with their 3D counterparts, 2D zeolites possessed several advantages like framework robustness, high thermal stability and tunable hydrophilicity/hydrophobicity. The preliminary work on plate-like MCM-22/silica composite membranes presented unprecedented opportunities of 2D zeolite membranes for facile and energy-efficient separation [19,20]. Nevertheless, preparation of high performance 2D zeolite membranes has been hindered by 1) the difficulty in delamination of single-unit-cell thick nanosheets and 2) the rigid framework structure, which inevitably led to the formation of interlayer defects. A breakthrough in 2D zeolite membrane fabrication stemmed from the successful delamination of MFI-type zeolites by designing a *di*-quaternary ammonium-type surfactant $C_{22}H_{45}$-$N_1(CH_3)_2$-C_6H_{12}-$N_1(CH_3)_2$-C_6H_{13} (called $C_{22\text{-}6\text{-}6}$) [21,22], which led to the formation of single-unit-cell 2 nm thick MFI nanosheets.

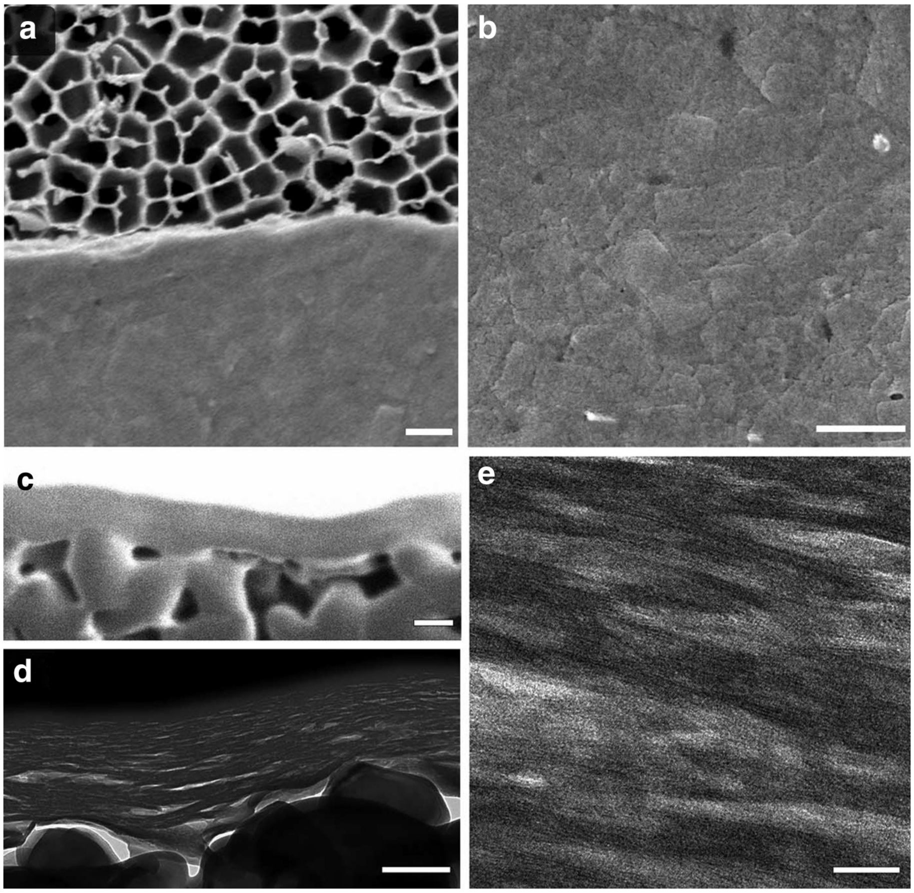

Fig. 2. SEM images of top view of coated MFI nanosheets on a a) AAO and b) porous α-Al_2O_3 substrates; c) FIB and d, e) TEM images of the cross section of MFI coatings. Scale bars: a–d), 200 nm; (e), 20 nm.
(Reproduced with permission [3]. Copyright 2011, American Association for the Advancement of Science.)

2.1.1. 2D MFI zeolite membrane

Based on the above-mentioned study, M. Tsapatsis further conducted a pioneering work on fabrication of 2D zeolite membranes by first exfoliation of multi-lamellar MFI zeolite precursors *via* melt blending with polystyrene followed by their restacking on porous α-alumina substrates *via* simple filtration of exfoliated aqueous suspensions (Fig. 2) [3]. Nevertheless, substantial nanometer-sized gaps existed between neighboring MFI nanosheets so that prepared 2D MFI zeolite membranes did not show any selectivity for *p*-/*o*-xylene mixtures. As a result, an additional mild secondary growth step was required to amend gaps between neighboring MFI nanosheets. Later this process was further improved in the following aspects: 1) Structure-directing agents (SDAs) were mildly removed with a piranha solution ($H_2O + H_2SO_4$) leading to an enhanced dispersion in water so that interlayer gaps existing between MFI nanosheets were anticipated to be reduced [23]. 2D MFI membranes were then prepared by re-self-assembly of uniformly dispersed MFI nanosheets in aqueous solution *via* simple vacuum filtration, showing an *n*-/*i*-butane selectivity of 5.4, which was a clear indication of the dominance of molecular sieving mechanism. 2) Floating-particle coating method was employed for facile deposition of single-unit-cell thick monolayer MFI nanosheets, which served as seed layers, on porous substrates [24]. After facile secondary growth, an ultra-high *p*-/*o*-xylene selectivity (>10000) was achieved. 3) A gel-less secondary growth method was developed for facile elimination of interlayer gaps between sub-100 nm-thick MFI-nanosheet seed layers [25]. Instead of conventional hydrothermal synthesis, in this study MFI-nanosheet seed layers were first impregnated with dilute aqueous TPAOH solution followed by simple thermal treatment under given conditions. Underlying 100 nm-thick silica buffer layers were served as the silica source. This method not only enabled reduction in the manufacturing costs but also enhanced the scale-up reproducibly.

It was noticed that conventionally 2D MFI nanosheets were prepared with the top-down method, which was time-consuming, costly and low-yield. Very recently M. Tsapatsis scored a further breakthrough in fabrication of 2D zeolite nanosheets *via* the bottom-up approach with improved yield and lower cost (Fig. 3) [26]. In this study, a nanocrystal-seeded growth method triggered by a single rotational intergrowth was developed to produce integrated 5 nm (2.5 single-unit-cell-thick) zeolite nanosheets. These high-aspect-ratio nanosheets allowed facile fabrication of thin defect-free 2D MFI nanosheet seed layers, which were further evolved into high-flux and ultra-selective MFI membranes after secondary growth. Future efforts should be focused on development of facile methods for eliminating interlayer gaps existing between 2D MFI nanosheets.

2.1.2. Other 2D zeolite membrane

AMH-3 is a kind of layered silicate with three-dimensional microporosity (eight-membered rings) within the layers. Because the unique 3D microporosity within layers, AMH-3 has been considered as an ideal nanofiller of MMMs for efficient gas separation. M. Tsapatsis first prepared swollen derivative of AMH-3 by a novel procedure involving sequential intercalation of dodecylamine after ion exchange in the presence of amino acid [27]. Further incorporation of swollen AMH-3 into polybenzimidazole (PBI) matrix leads to a doubling of H_2/CO_2 ideal selectivity (R. T.) than that of pure PBI membranes due to additional molecular sieve properties of swollen AMH-3 nanofillers (Fig. 4) [27]. In addition, similar ideal selectivity was observed with higher loadings (*e.g.*, 14%) of proton-exchanged AMH-3 particles indicating that diffusion of H_2 was faster than CO_2 in AMH-3-derived silicates. Besides PBI, post-modified AMH-3 nanofillers were further incorporated in cellulose acetate (CA) and Polysulfone (PSf) matrices, resulting in significant improvements in gas separation performances [28].

JDF-L1 represents a layered titanosilicate exhibiting with an in-plane pore size ~0.3 nm, making them superb candidates for separating H_2-containing gas mixtures. J. Coronas and C. Staudt first prepared JDF-L1-copolyimide MMMs with disaggregated plate-like JDF-L1 as nanofillers [29]. Gas permeation results indicated that horizontal dispersion of JDF-L1 particles into the polymer matrix was beneficial for improving the H_2/CH_4 selectivity, owing to the elongated diffusion path for CH_4. Further exfoliation of JDF-L1 was achieved by melt compounding commercial PSf together with swollen JDF-L1 processed with PSf [30]. Prepared JDF-L1-PSf MMMs showed simultaneous improvement of H_2 permeability and H_2/CH_4 selectivity, which was attributed to the incorporation of highly dispersed exfoliated JDF-L1 nanosheets. It was noted that in addition to a single JDF-L1 nanofiller, J. Coronas further confirmed that combination of both JDF-L1 and calcined MCM-41 fillers for MMMs gave rise to a synergy effect favoring uniform dispersion of fillers so that both higher H_2 permeability and H_2/CH_4 selectivity were achieved in comparison with pure polymer membranes [31].

In addition to above-mentioned zeolite framework types, 2D MWW zeolite nanosheets with a free internal diameter close to 0.71 nm delimited by 12 MR have been prepared by repeated exfoliation of the corresponding layered precursor ITQ-1 [32]. Although 2D MWW zeolites may not be ideal for precise molecular sieving due to their relatively large pore aperture, they may serve as high performance catalytic membrane reactors upon incorporation of catalytic active species (like Ti) into the framework. For instance, X. S. Chen prepared dense and well-intergrown 2D Ti-MWW zeolite membranes on porous mullite substrates by secondary hydrothermal synthesis [33]. Prepared Ti-MWW zeolite membranes exhibited excellent catalytic activity for the phenol hydroxylation by pervaporation, and the phenol conversion and dihydroxybenzene selectivity reached 22.94% and 98.33% at 323 K, respectively.

2.2. 2D MOF membrane

Owing to the high flexibility in both pore apertures and functionality, MOFs in the form of membranes have offered unprecedented opportunities for energy-efficient gas/liquid separation. Conventionally MOF

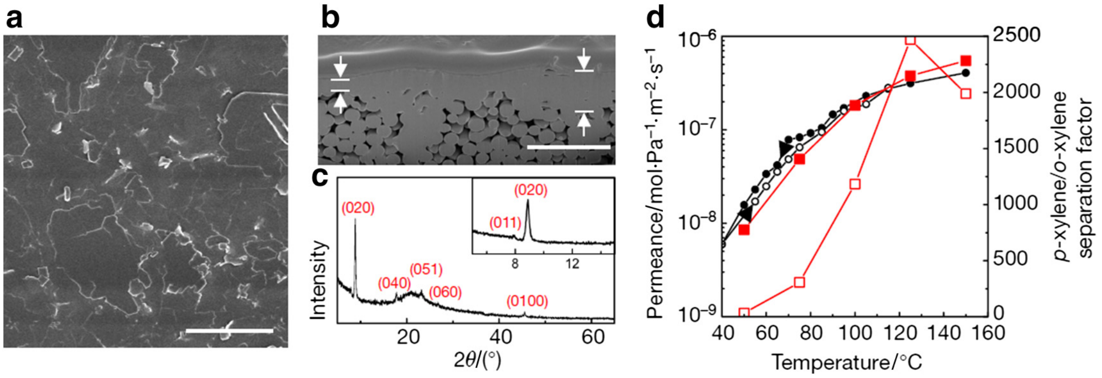

Fig. 3. a, b) Top and cross-sectional views of MFI membranes prepared by gel-free intergrowth of MFI nanosheets. Scale bars: 2 μm; c) XRD pattern for the MFI membrane; d) *p*-xylene permeance and selectivity for MFI membrane.
(Reproduced with permission [26]. Copyright 2017, Nature Publishing Group.)

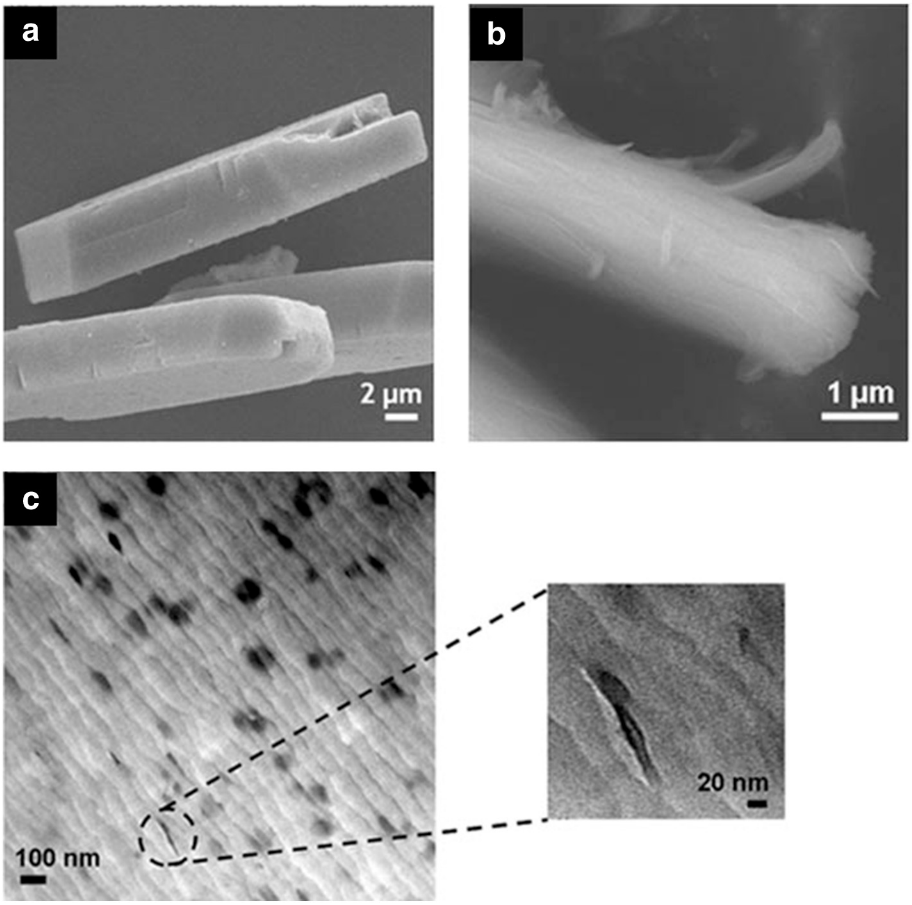

Fig. 4. SEM images of a) original and b) swollen AMH-3; c) TEM images of a cross section from 3 wt% swollen AMH-3 nanocomposite. (Reproduced with permission [27]. Copyright 2008, Wiley-VCH.)

materials employed in membrane fabrication dominantly possess a 3D framework. In contrast, membranes constructed from 2D layered MOFs have been rarely explored. The difficulty in fabricating high performance 2D MOF membranes lies in the lack of facile methods for exfoliation of bulk MOF materials while maintaining morphological and functional integrity of exfoliated 2D MOF nanosheets. Moreover, facile methods for re-assembly of exfoliated MOF nanosheets into defect-free ultra-thin 2D MOF membranes are yet to be developed.

2.2.1. 2D MOF membrane in pure form

Pioneering work on the fabrication of 2D MOF membranes was conducted by W. S. Yang and Y. S. Li who first prepared 1-nm-thick 2D $[Zn_2(bim)_4]$ nanosheets and constructed ultra-thin (<10 nm) 2D $[Zn_2(bim)_4]$ membranes with unprecedented H_2/CO_2 separation performance (Fig. 5) [34]. In the first step, monodispersed $[Zn_2(bim)_4]$ nanosheets were prepared by exfoliation with a novel soft-physical process involving low speed wet ball-milling and ultra-sonication-assisted exfoliation. Owing to the structural flexibility, theoretical 0.21 nm-sized pores within $[Zn_2(bim)_4]$ nanosheets permitted fast permeation of H_2 while other gases with larger kinetic diameters were excluded. In the next step, a hot-drop coating technique was developed for disordered stacking of 2D $[Zn_2(bim)_4]$ nanosheets on porous α-Al_2O_3 substrates. Under optimized operating conditions, a H_2/CO_2 selectivity ~300 with a H_2 GPU of ~3000, which had by far exceeded the latest Robeson upper-bound for the H_2/CO_2 gas pair, was achieved. Very recently W. S. Yang further disintegrated bulky $[Zn_2(Bim)_3]$ into lamellar amphiprotic MOF nanosheets *via* a modified soft physical exfoliation method [35]. Consequently sub-10 nm-thick ultrathin membranes were prepared with the previously developed hot-drop coating method and demonstrated remarkably high H_2/CO_2 separation performance.

In a similar manner, D. Zhao prepared ultra-thin MAMS-1 membranes composed of 2D MAMS-1 nanosheets first by mild exfoliation of layered precursors *via* freeze–thaw approach in suitable solvent systems, followed by aligning large MAMS-1 nanosheets onto porous AAO substrates *via* a hot-drop casting method (Fig. 6) [36]. Most notably, membranes derived from well-aligned MAMS-1 nanosheets showed an unprecedented reversed thermos-switchable H_2 permeability, which was attributed to the structural flexibility of MAMS-1 nanosheets.

Besides exfoliation, H. T. Wang further prepared preferentially *b*- and *c*-oriented 2D bulky ZIF-L membranes by conventional solvothermal growth [37]. ZIF-L possessed a cushion-shaped cavity between nanosheets with a dimension of 0.94 nm × 0.7 nm × 0.53 nm. Owing to their relatively large cavity size and considerable membrane thickness (~5 μm), prepared 2D layered ZIF-L membranes did not show superior separation performance (like H_2/CO_2 and H_2/N_2) over traditional 3D MOF membranes. To further reduce the membrane thickness, G. L. Zhang and E. Zeng developed a novel gel-vapor deposition (GVD) method, which combined sol–gel coating with vapor deposition, for facile and scalable production of ultra-thin (~17 nm) ZIF-8 membranes [38]. Prepared membranes showed considerably high selectivities (3126 and 73.4) for H_2/C_3H_8 and C_3H_6/C_3H_8 mixtures, respectively.

Besides gas separation, 2D MOF materials could further serve as ideal candidates for high performance NF membranes. For instance, L. Hong utilized polycationic polymers (*i.e.*, PEI or PDDA) to regulate the assembling of 2D Zn-TCP(Fe) nanosheets through the cross-linking between polycation coils and the periphery carboxylic groups of 2D Zn-TCP(Fe) nanosheets [39]. Owing to the well-aligned channels for efficient water purification, prepared polycation-regulated 48 nm-thick 2D Zn-TCP(Fe) membranes showed ultrahigh permeance of 42430 $L \cdot m^{-2} \cdot h^{-1} \cdot MPa^{-1}$

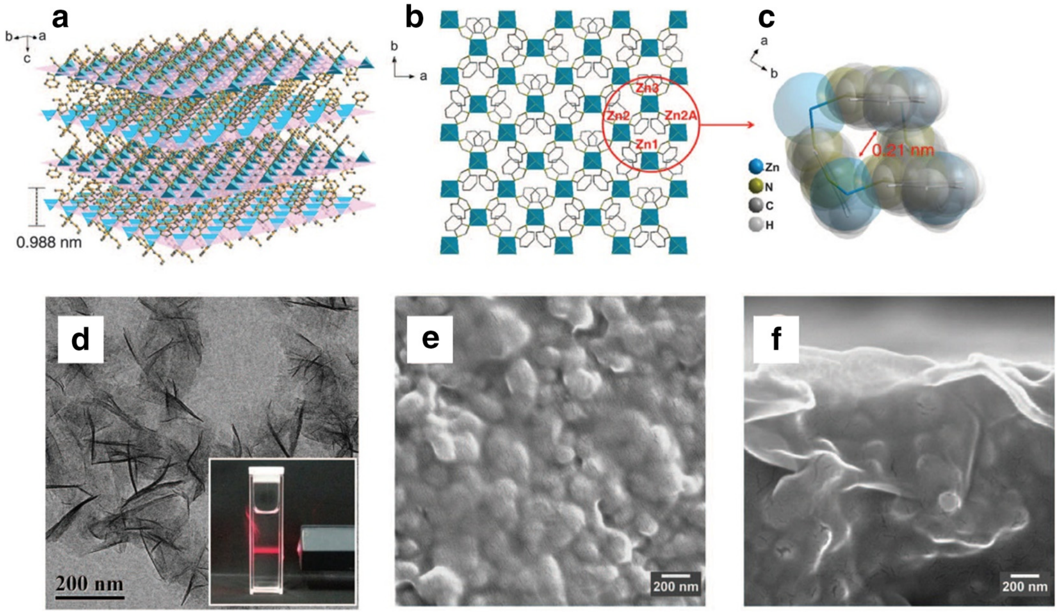

Fig. 5. a) Architecture of layered MOF precursor; b) illustration of the grid-like structure of $[Zn_2(bim)_4]$ nanosheets; c) space-filling representation of $[Zn_2(bim)_4]$ nanosheets; d) TEM image of $[Zn_2(bim)_4]$ nanosheets; e) top and f) cross-section of a $[Zn_2(bim)_4]$ layer on α-Al_2O_3 substrate.
(Reproduced with permission [34]. Copyright 2014, American Association for the Advancement of Science.)

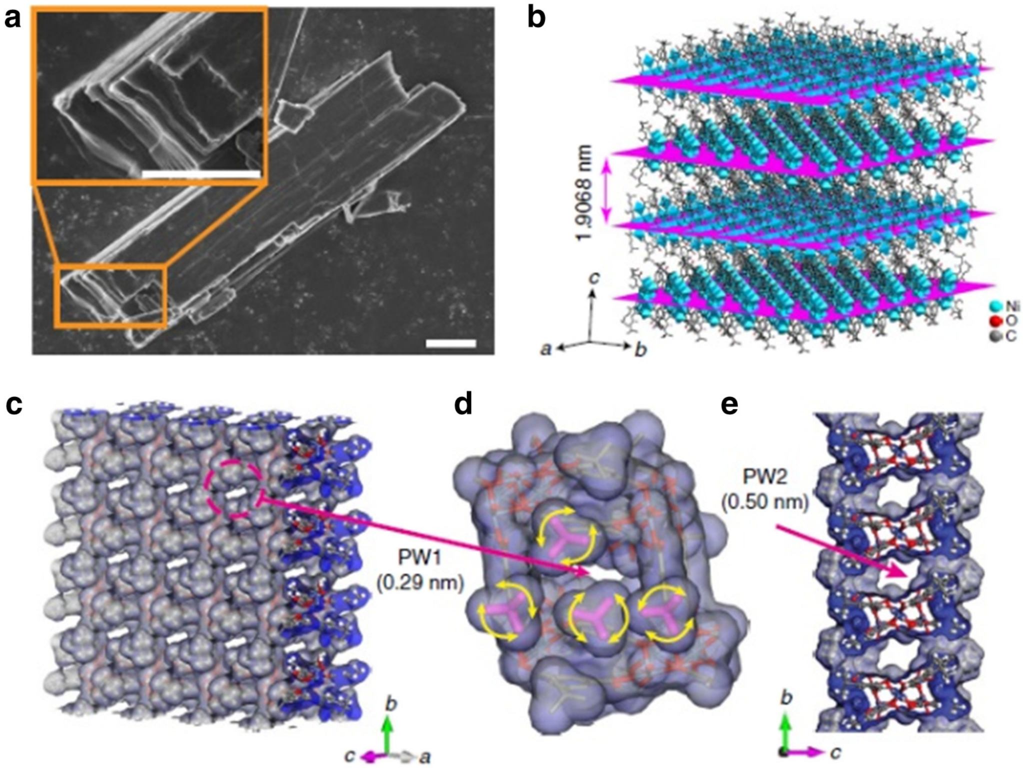

Fig. 6. a) The SEM image of layered MAMS-1 crystals. Scale bars: 5 mm; b) crystal structure of MAMS-1; c) tilted vertical view of ab plane in MAMS-1 monolayer; d) amplified view of PW1 gated by two pairs of tert-butyl group; e) view along *a*-axis of MAMS-1 monolayer.
(Reproduced with permission [36]. Copyright 2017, Nature Publishing Group.)

and excellent rejection rates (>90%) for organic dye with size larger than 0.8 nm × 1.1 nm.

2.2.2. 2D MOF membrane in a mixed-phase form

Besides in a pure form, 2D layered MOF nanosheets could further integrate with other selective materials (like 3D MOFs, GO and polymers) to form highly compatible 2D MOF-based mixed-phase membranes. For instance, J. Gascon developed a bottom-up synthesis strategy for the fabrication of dispersible [Cu(1,4-bdc)]-polyimide MMMs (Fig. 7) [40]. Incorporating 5 nm-thick MOF nanosheets into polymer matrices endowed resultant MMMs with outstanding CO_2/CH_4 selectivity (~90). This could be attributed to a superior occupation of the membrane cross-section by MOF nanosheets as compared with bulk crystals, which improved the accuracy of molecular sieving and minimized non-selective permeation pathways. In a similar way D. Zhao prepared MMMs by blending PBI with $[Cu_2(ndc)_2(dabco)]_n$ with diverse morphologies (bulk crystal, nanocube and nanosheet) [41]. Gas permeation tests indicated that the morphology of MOF fillers was closely associated with their separation performance. The best H_2/CO_2 separation performance was achieved in nanosheet-PBI MMMs due to a preferential exposure of the small pore size of the (001) crystal plane (0.37 nm × 0.37 nm) towards the gas concentration gradient. In addition to PBI, $[Cu_2(ndc)_2(dabco)]_n$ nanosheets were further incorporated in PIM-1 polymers showing excellent CO_2/CH_4 separation performance [42]. Besides gas separation, F. S. Pan further incorporated ZIF-L sheets and ZIF-8 nanocrystals into sodium alginate (SA) matrix for pervaporation dehydration of ethanol [43]. ZIF-L-SA MMMs displayed superior separation performance than ZIF-8-SA MMMs, owing to the ordered water channels for rapid transport of water molecules and the desirable molecular sieving effect. Furthermore, prepared MMMs exhibited excellent swelling resistance and thermal stability.

Besides polymers, 2D MOF nanosheets could also easily couple with other MOF materials or GOs to form 2D MOF-based composite separation membranes. For instance, Kang developed a novel method involving the employment of 2D layered ZIF-L as seed crystals for the epitaxial growth of continuous ZIF-8 layers which ultimately led to the formation of ZIF-L-ZIF-8 composite membranes [44]. This approach guaranteed effective incorporation of ZIF-L within the ZIF-8 matrix with a high volume fraction of ZIF-L (~28%). Compared with pure ZIF-8 membranes, ZIF-L–ZIF-8 composited membranes exhibited a 3-fold enhancement in H_2 permeability as well as a decent increase in H_2/CO_2 selectivity. The superior separation performance of ZIF-L–ZIF-8 composite membranes was attributed to the intrinsically high diffusivity of ZIF-L for H_2.

2.3. 2D COF membrane

2D COFs represent a novel class of crystalline nanoporous materials with highly ordered honeycomb networks. Recent studies indicated that bulk 2D COFs could be further exfoliated into ultrathin 2D COF nanosheets, therefore providing unprecedented opportunities for industrial applications in diverse occasions.

C. L. Zhong first proposed the application of a monolayer triazine-based CTF-0 membrane for effective separation of He and H_2 purification based on first-principle calculations [45]. Relying on diffusion barrier calculations, it was demonstrated that a monolayer CTF-0 membrane exhibited exceptionally high He and H_2 selectivity over Ne, CO_2, Ar, N_2, CO, and CH_4 with superior He and H_2 permeabilities. In addition to CTF-0, C. L. Zhong further conducted a systematic study on the CO_2/N_2 separation performance of a series of designed few-layered ultrathin triazine-based CTF-1 membranes [46]. Simulation results indicated that regulating the size of interlayer passages between stacked 2D COF nanosheets led to the formation of diverse ultra-thin 2D COF membranes with distinct separation performances. Moreover, controlling the stacking mode between 2D COF nanosheets enabled to construct a favorable energetic microenvironment for achieving superior separation performance.

G. Li and T. Tsuru successfully fabricated uniform and ultra-thin 2D COF-1 membranes with exfoliated microporous COF-1 nanosheets as building blocks (Fig. 8) [47]. Precise manipulation of the membrane microstructure resulted in formation of ultra-permeable COF-1 membranes due to the ultrafast diffusion of guest molecules through interlayer gaps between assembled COF nanosheets as well as outstanding thermal stability due to the robust covalent bonds in the COF-1 framework.

D. Zhao successfully synthesized water-stable 2D NUS-2 and NUS-3 with excellent thermal stability (~300 °C) and resistance towards hydrolysis under both neutral and acidic conditions [48]. Bulky NUS-2 particles were further exfoliated into monodispersed nanosheets under sonication and stirring, and then blended with Ultem and PBI into MMMs with excellent compatibility and mechanical properties. Compared with the pure polymer membranes, prepared 20 wt% NUS-2@PBI MMMs exhibited enhanced H_2 gas permeability and H_2/CO_2 selectivity surpassing the 2008 Robeson upper bound.

In addition to 2D COF-based MMMs, C. L. Zhong further proposed a GO-assisted layer-by-layer restacking method to fabricate ultrathin

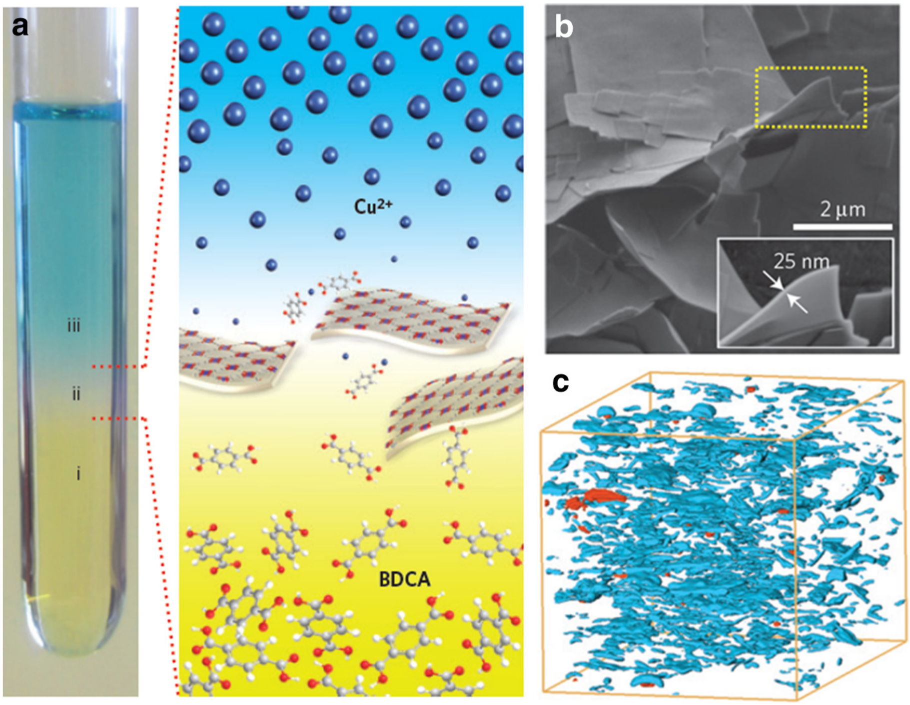

Fig. 7. a) Schematic illustration of the spatial arrangement of different liquid layers during the synthesis of CuBDC MOF nanosheets; b) the SEM image of CuBDC MOF nanosheets; c) surface-rendered views of segmented FIB–SEM tomograms for nanosheet CuBDC MOF-polyimide MMMs.
(Reproduced with permission [40]. Copyright 2015, Nature Publishing Group.)

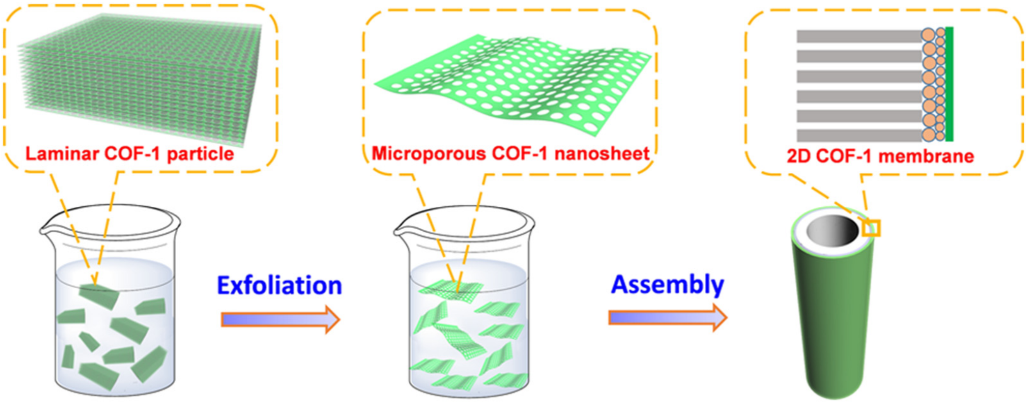

Fig. 8. Schematic illustration of the preparation of a COF-1 membrane via the assembly of exfoliated COF-1 nanosheets. (Reproduced with permission [47]. Copyright 2017, American Chemical Society.)

GO–CTF-1 composite membranes for gas separation [49]. Favorable functional group interactions between GO and CTF-1 nanosheets led to the formation of 100 nm-thick GO–CTF-1 composite membranes exhibiting high H_2 permeance as well as competitive H_2/CO_2 selectivity.

Besides gas separation, very recently H. Meng and J. Caro prepared defect-free 2D imine-linked 400 nm-thick COF-LZU1 membranes by *in situ* solvothermal growth [50]. Prepared membranes exhibited unprecedented water permeance (~760 $L \cdot m^{-2} \cdot h^{-1} \cdot MPa^{-1}$) as well as considerable rejection rates (>90%) for dyes larger than 1.2 nm. Long-time operation further confirmed the outstanding water stability of prepared membranes.

2.4. 2D LDH membrane

LDHs are representative of anionic clays composed of positively charged brucite-like 2D sheets, charge compensating anions and solvation molecules located in interlayer galleries. Compositional flexibility and gallery height adjustability of LDHs give rise to a functional diversity. Furthermore, microstructures of LDHs can be easily tuned by changing the synthetic strategy, therefore making them superb candidates of high-performance separation membranes and complementary buffer layers.

2.4.1. LDH-based separation membrane

By employing a vacuum-suction approach, Tsotsis took an initial step in fabrication of MgAl–CO_3 LDH-based separation membranes showing an ideal CO_2/N_2 selectivity of 35 after repairing cracks and defects by silicone coating [51,52]. In the next step, an electrophoretic deposition (EPD) technique was employed to deposit plate-like LDHs on porous α-Al_2O_3 substrates. Prepared LDH membranes showed preferred selectivity towards CO_2 [53].

Y. Liu and J. Caro further extended the utilization of LDH membranes in H_2 purification. Well-intergrown NiAl–CO_3 LDH membranes could be successfully prepared on mesoporous γ-Al_2O_3 substrates by facile *in situ* hydrothermal growth (Fig. 9) [54]. XRD pattern further indicated a uniform gallery height of 0.31 nm, which was smaller than kinetic diameters of most gas molecules. Correspondingly, the H_2/CH_4 SF of prepared NiAl–CO_3 LDH membranes reached ~80. In a further study, it was found that the concentration of CO_2 dissolved in the precursor solution played a critical role in controlling the preferred orientation of LDH membranes: Trace amount of CO_2 induced formation of *ab*-oriented 0.6 μm-thick LDH membranes, whereas over-saturated CO_2 gave rise to the formation of randomly oriented 5 μm-thick LDH membranes [55]. Although both LDH membranes showed clear size-based selectivity, randomly oriented LDH membranes showed much higher H_2 selectivity possibly due to reduced mesoscopic defects. Compared with conventional exfoliation–restacking process, nucleation of LDH crystallites, their attachment to substrates and final formation of compact LDH membranes could be completed in one step.

It was noted that besides NiAl–CO_3 LDH membranes, with a similar method, Y. Liu and J. Caro further prepared well-intergrown ZnAl–NO_3 LDH membranes with the gallery height of 0.42 nm, which was larger than H_2, CO_2, N_2 and CH_4 [55]. Therefore, SF of H_2/CO_2, H_2/N_2 and H_2/CH_4 gas pairs on ZnAl–NO_3 LDH membranes was considerably lower than that of NiAl–CO_3 LDH membranes.

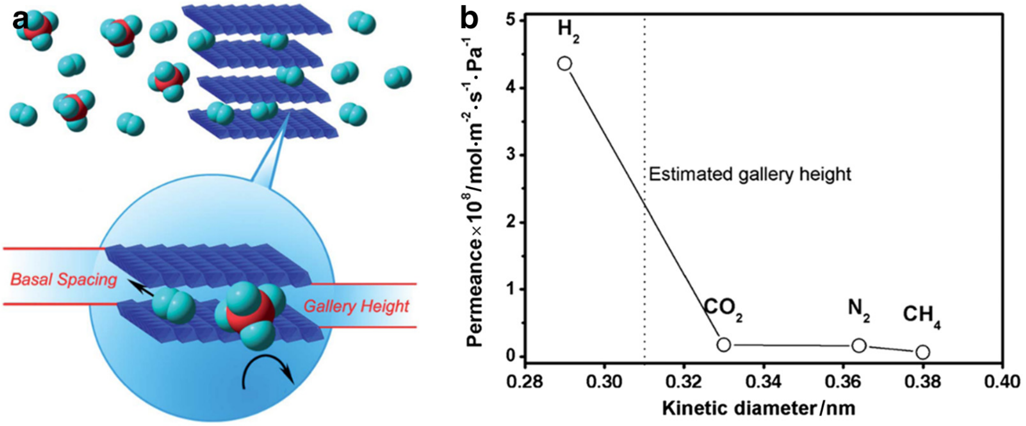

Fig. 9. a) Schematic elucidation of the concept of selective molecular sieving through their interlayer galleries; b) permeances of the single gases through NiAl–CO_3 LDH membranes. (Reproduced with permission [54]. Copyright 2014, The Royal Society of Chemistry.)

Besides in pure form, Y. Liu and J. Caro further successfully prepared ZIF-8–ZnAl–NO_3 LDH composite membranes in one step by partial conversion of ZnAl–NO_3 LDH precursor membranes (Fig. 10) [56]. Partial dissolution of ZnAl–NO_3 LDHs led to reduced framework density and therefore enhanced H_2 permeance. Moreover, since there existed both ZIF-8 and ZnAl–NO_3 LDH selective layers, prepared composite membranes showed significantly enhanced H_2/CH_4 selectivity.

In addition to interlayer gallery-based separation mechanism, relying on the unique "memory effect" of LDHs, recently S. C. Wang further proposed a calcination–reconstruction method to prepare MgAl–CO_3 LDH-based facilitated transport membranes by designing high-speed CO_2 facilitated transport channels [57]. Prepared membranes displayed excellent CO_2/N_2 permselectivity (268) and ultra-high CO_2 permeance (5693 GPU) by *in situ* reconstruction of calcined MgAl–CO_3 LDH fillers as high-speed facilitated transport channels. In addition, both ZnAl–CO_3 and NiAl–CO_3 LDH fillers also enabled to improve the CO_2/N_2 selectivity to a certain extent.

2.4.2. LDH-based complementary buffer layer

LDHs could also serve competent complementary buffer layers for fabrication of high performance MOF membranes, relying on the high length-to-width ratio, rich surface functionality and unique thermal properties. For instance, with a simple *in situ* hydrothermal method, vertically aligned MgAl–CO_3 LDH networks could be introduced on α-Al_2O_3 substrates [58]. Consequently, ZIF-8 seeds were uniformly embedded into the LDH network by dip-coating. Owing to the hindrance from adjacent LDH walls, trapped ZIF-8 seeds were firmly attached to substrates and would not easily peel off. Finally, well-intergrown ZIF-8 membranes exhibiting excellent H_2 permselectivity were prepared after epitaxial growth.

In addition to MgAl–CO_3 LDHs, it was found that vertically aligned ZnAl–CO_3 LDH buffer layers could be further *in situ* synthesized on γ-Al_2O_3 substrates (Fig. 11) [59]. The high length-to-width ratio and rich surface functionality of LDH grains led to the formation of well-intergrown ZIF-8 membranes by simple *in situ* solvothermal growth. To sum up, LDH complementary buffer layers have guaranteed

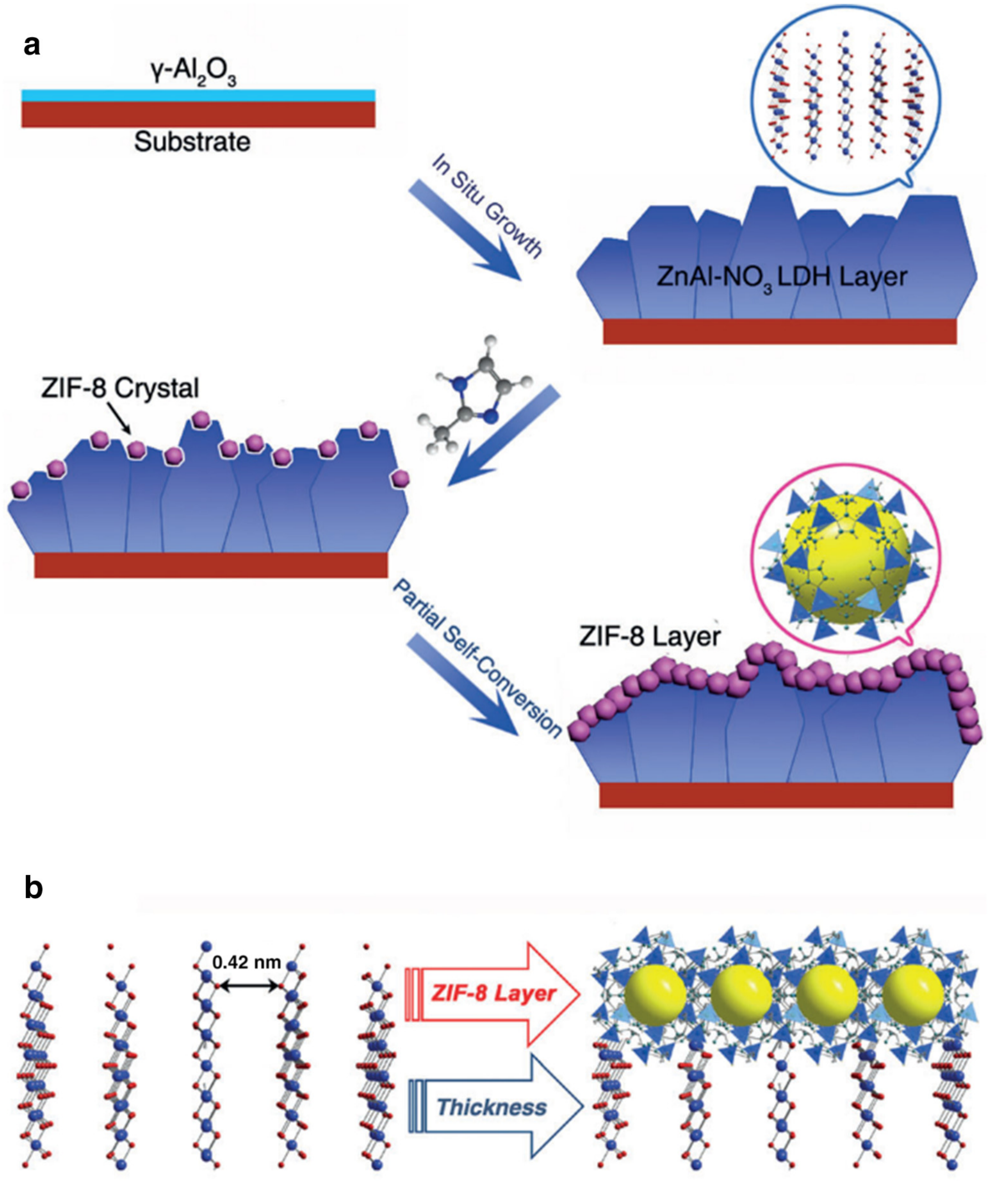

Fig. 10. a) Schematic illustration of partial self-conversion of a ZnAl–NO_3 LDH precursor layer into a ZnAl–NO_3–ZIF-8 membrane; b) structural evolution of the ZnAl–NO_3 LDH membrane after the solvothermal treatment with 2-methylimidazole.
(Reproduced with permission [56]. Copyright 2015, Wiley-VCH.)

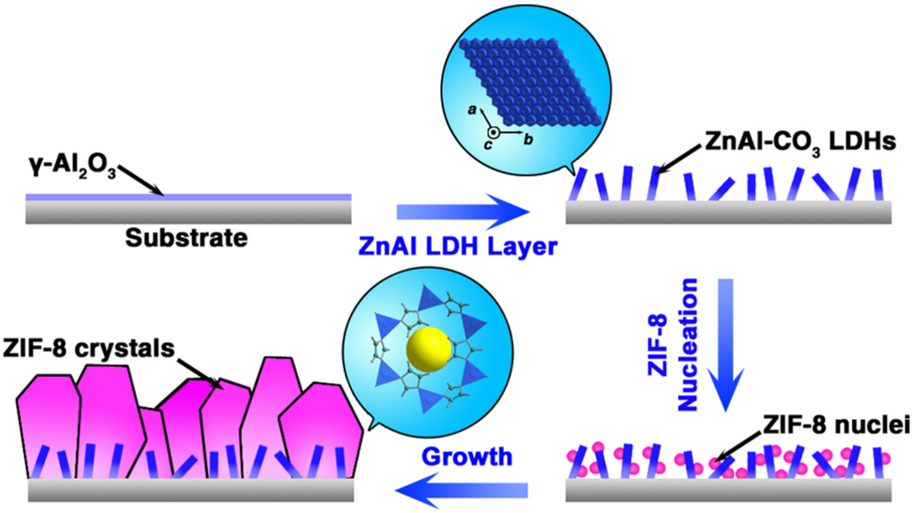

Fig. 11. Schematic illustration of *in situ* solvothermal growth of ZIF-8 membrane on a ZnAl-LDH buffer layer-modified γ-Al_2O_3 substrate. (Reproduced with permission [59]. Copyright 2014, American Chemical Society.)

facile formation of well-intergrown MOF membranes with ideal gas selectivity.

The unique thermal behavior of LDHs enabled to improve the separation performance of MOF membranes further. Prior to solvothermal treatment with the ligand 2-methylimidazole (2-mIm), H_2-selective ZnAl–NO_3 LDH precursor membranes were calcined at 350 °C, generating nano-sized ZnO buffer layers serving as sole metal sources of ZIF-8. H_2/CH_4 selectivity of prepared ZIF-8 membranes reached 83.1, which was by far the highest value ever reported for pure ZIF-8 membranes possibly due to the framework rigidization caused by underlying nano-sized ZnO buffer layers [60].

2.5. TMDC membrane

TMDCs are a representative of layered compounds with the formula MX_2 showing a “sandwich” structure with two chalcogen atomic layers separated by a transition metal atomic layer [61]. The weak van der Waals interlayer interaction permits facile intercalation of foreign molecules into the interlayer gallery. Recent decades witnessed significant attention paid to TMDC materials due to their unique layered structure and the presence of *d*-electrons in transition metals. Being analogous to LDHs, the existence of open controllable interlayer spaces enabled selective permeation of guest molecules through TMDC-based separation membranes. Among diverse TMDC materials, MoS_2 and WS_2-based separation membranes have been most extensively studied and shown great potential for efficient gas separation, pervaporation and desalination. In addition, drilling in-plane nanopores with controllable structure and chemical environment, although still in its infancy, has shown great promise in membrane-based separation.

Taking MoS_2, one of the most extensively studied TMDC materials as an example, although there existed few in-plane nanopores within a single MoS_2 nanosheet, results from molecular dynamics simulations have indicated that even a single-layer MoS_2 nanosheet may exhibit unprecedented performance in gas separation and desalination upon

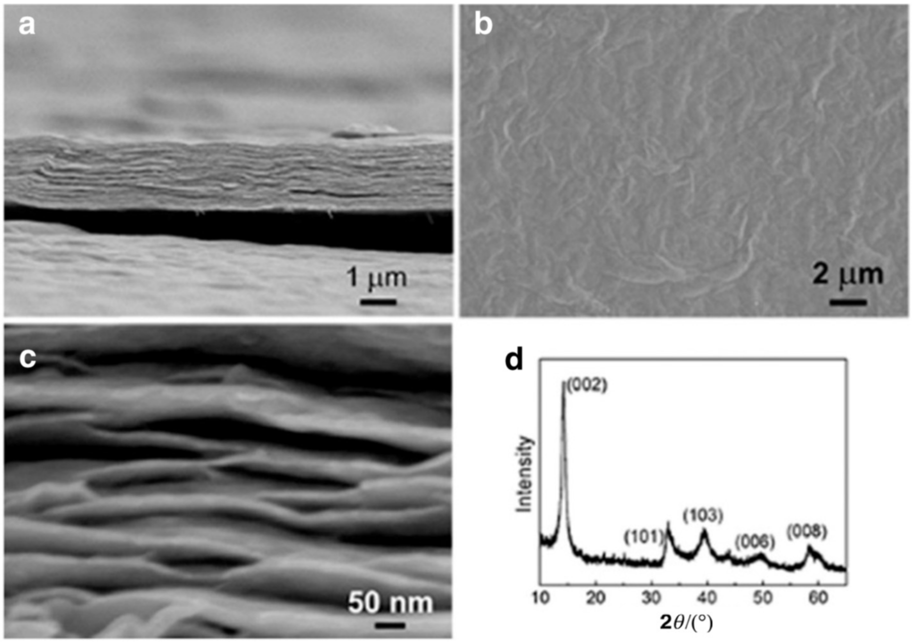

Fig. 12. a) Cross-sectional, b) top, and c) high-magnification cross-sectional SEM images of prepared MoS_2 membranes; (d) XRD pattern recorded from the sample. (Reproduced with permission [65]. Copyright 2013, The Royal Society of Chemistry.)

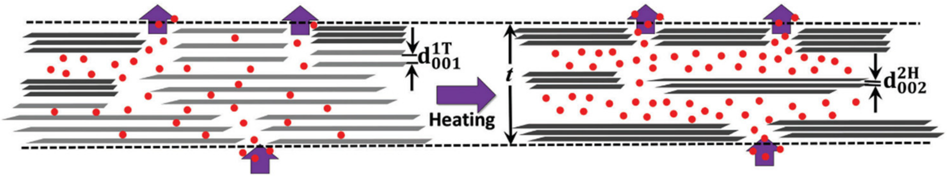

Fig. 13. Schematic illustration of gas permeation pathway across MoS_2 membranes before and after heating at 160 °C. (Reproduced with permission [67]. Copyright 2016, The Royal Society of Chemistry.)

assuming that in-plane nanopores with controlled shape, size and functionality could be drilled in a large scale [62–64].

At present interlayer gallery-based separation remained the dominant separation mechanism for MoS_2-based membranes. For instance, X. S. Peng fabricated 1.7 μm-thick MoS_2 membranes by self-assembling atom-thick MoS_2 nanosheets *via* vacuum filtration (Fig. 12). Prepared MoS_2 membranes exhibited a water permeance 3–5 times higher than GO membranes without sacrificing the rejection ratio (89%) for Evans blue [65].

In addition to desalination, J. Jin further prepared AAO-supported 17 nm-thick MoS_2 membranes by simple vacuum filtration for gas separation [66]. Nevertheless, prepared membranes exhibited poor H_2/CO_2 selectivity (~3), implying that substantial non-selective defects existed. Therefore, facile methods for elimination of interlayer defects were yet to be developed. In a further study conducted by M. Eswaramoorthy, 500 nm-thick MoS_2 membranes were prepared *via* vacuum filtration of 1T MoS_2 solution (Fig. 13) [67]. Surprisingly, prepared 1T MoS_2 membranes exhibit unprecedented H_2 permeability (1175 barrer) as well as H_2/CO_2 selectivity (8.29). Moreover, a significant increase in gas permeability was observed at higher operating temperature (>160 °C) due to the phase transition of MoS_2 from 1T to the 2H.

In contrast to the pursuit of sub-micrometer thickness, H. G. Park prepared freestanding 20 μm-thick stacked MoS_2-platelet membranes by simple vacuum filtration [68]. A clear size-based selectivity for organic vapor molecules was observed, which could be interpreted as mechanistic interplay of steric hindrance, compatibility with the 2D hydrogen bonding network of water and electrostatic interaction. To further associate the desalination performance of MoS_2 membranes with their nanochannel size, X. M. Bao discovered that fully hydrated MoS_2 membranes maintained a 0.9 nm gallery height, and the low hydraulic resistance of smooth and rigid nanochannels significantly contributed to the high water flux; in contrast, completely dehydrated MoS_2 membranes maintained a 0.3 nm free spacing which was almost impermeable to water [69].

Post-modification represented an effective method to achieve further performance enhancement of MoS_2 membranes. M. A. Bissett produced 5 μm-thick MoS_2 membranes with high rejection rate (~99%), high water fluxes (5 times higher than GO membranes with similar thickness) and long-term operation stability by simple immersion of MoS_2 precursor membranes in dye solutions under deliberately controlled conditions [70]. Post-modification of MoS_2 nanosheets with charged dye molecules led to a change in the surface charge near the membrane interface, which unambiguously contributed to the enhanced desalination performance. In addition to charged dyes, X. S. Peng further reported post-modification of 2D channels within MoS_2-laminated membranes with an ionic liquid, [BMIM][BF_4] *via* the infiltration process (Fig. 14) [71]. Compared with the bulk [BMIM][BF_4], MoS_2-supported ionic liquid membrane exhibits superior CO_2 permeance and CO_2/N_2 permselectivity, which was attributed to the nanoconfined [BMIM][BF_4] enabling preferential diffusion of CO_2 molecules.

Besides in pure form, delaminated MoS_2 nanosheets could be further incorporated into polymer matrices for construction of high performance MMMs. Y. T. Zhang first used MoS_2 nanosheets as an inorganic nanofiller of Pebax 1657 matrix for CO_2/N_2 separation [72]. A simple drop-coating–evaporation approach was employed to prepare the MoS_2–Pebax MMMs. Both permeability (64 barrer) and selectivity (93) of the MMMs had far exceeded pristine Pebax membranes. It was assumed that stronger adsorption energy of MoS_2 nanosheets to CO_2 than N_2 contributed to the enhancement of CO_2/N_2 selectivity. In addition to gas separation, Z. Y. Jiang further prepared delaminated MoS_2–Pebax MMMs for removal of thiophene from the *n*-octane/thiophene mixture, relying on the proper binding energy of thiophene molecule on the basal plane of MoS_2 nanosheets [73]. Under optimized conditions, prepared MMMs exhibited a permeation flux of 11.42 $kg\cdot m^{-2}\cdot h^{-1}$ with an enrichment factor of 9.11, which were both higher than that of pure Pebax membranes.

Being analogous to MoS_2 membranes, X. S. Peng further prepared WS_2 membranes composed of exfoliated WS_2 nanosheets *via* vacuum filtration

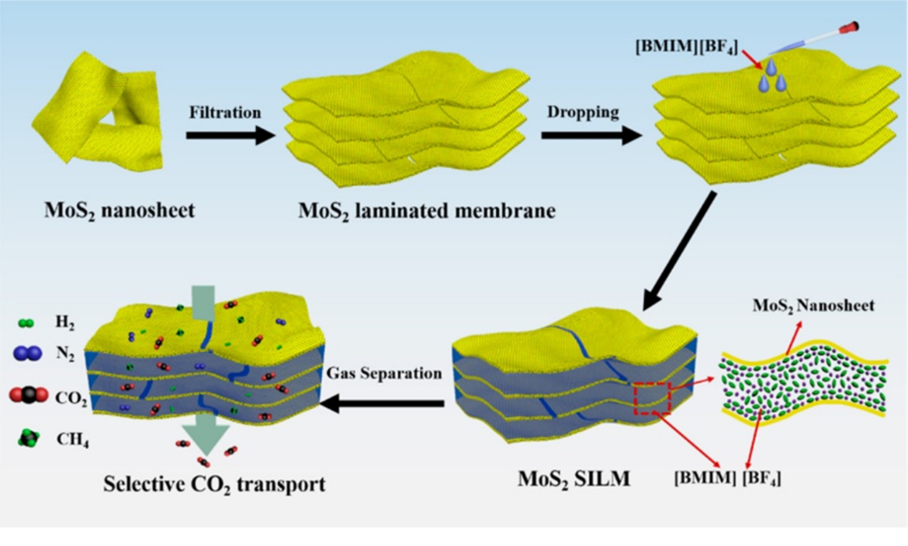

Fig. 14. Illustration of fabrication process of IL-impregnated MoS_2 membranes *via* infiltration. (Reproduced with permission [71]. Copyright 2017, American Chemical Society.)

[74]. Prepared membranes showed 2-fold enhancement in water permeance of MoS_2 laminar membranes with similar rejection rate. To enhance the water flux further, ultra-thin $Cu(OH)_2$ nanostrands were employed as hard templates to generate more fluidic channel networks, resulting in a 2-fold increase of the water flux without significantly degrading the rejection rate.

Besides in pure form, V. Bruggen further fabricated PES–WS_2 flat-sheet MMMs for Human Acid removal from aqueous solution *via* non-solvent induced phase separation (NIPS) [75]. A significant enhancement in the permeability was observed as a result of the incorporation of ultra-low fractions of nano-WS_2. Simultaneously, bother fouling resistance and solute rejection rate were remarkably enhanced.

2.6. MXene membrane

MXenes are a family of early transition metal carbides receiving increasing attention since their first discovery. $Ti_3C_2T_X$ as a representative of MXenes [76], was conventionally prepared from Ti_3AlC_2 precursors through a HF etching process. Owing to the framework flexibility, extraordinary structural stability, rich functionality, intrinsic surface hydrophilicity and excellent exfoliation capability, $Ti_3C_2T_X$ has offered unprecedented opportunities for membrane-based separation.

2.6.1. Pure MXene membrane

Y. Gogotsi conducted a pioneering study on MXene-based separation membranes [77]. Exfoliated 2D $Ti_3C_2T_X$ sheets were assembled into freestanding or supported membranes therefore demonstrating ultra-fast water flux and molecular sieving capability towards salts depending on both the hydration radius and charge of ions. Moreover, different from GO membranes, the ultra-fast water flow through MXene membranes was attributed to the presence of one or more H_2O molecule layers between $Ti_3C_2T_x$ layers in the wet state. To enhance the water flux further, H. H. Wang further prepared AAO-supported MXene membranes by filtration deposition during which colloidal $Fe(OH)_3$ nanocrystals were employed as the as distance holder (Fig. 15) [78]. Prepared MXene membranes exhibited unprecedented water permeance (>10000 $L\cdot m^{-2}\cdot h^{-1}\cdot MPa^{-1}$) while maintaining a high rejection rate (90%) for guest molecules (> 2.5 nm). Such high water permeance was interpreted as the following two aspects: First, nanometer-sized MXene sheets were employed instead of the traditional micrometer-sized MXene sheets so that transport pathways were greatly reduced. Second, intercalated Fe_3O_4 nanoparticles, which were subsequently removed by mild acid etching, were used as pillars to achieve larger interlayer distance and create more nanochannels. To improve the salt rejection ratio further, W. Q. Jin prepared ultra-thin (~60 nm) MXene membranes for pervaporation desalination [79]. Owing to unique 2D interlayer channels as well as intrinsic hydrophilicity, prepared MXene membranes showed excellent NaCl rejection capacity (99.5%), high water flux and excellent long-term stability.

Very recently the application of MXene membrane was further extended to gas separation. H. H. Wang fabricated $Ti_3C_2T_X$ membranes with uniformly aligned sub-nanometer interlayer galleries by using abundant functional groups on MXene nanosheets (Fig. 16) [80]. Both H_2 permeability and H_2/CO_2 selectivity of prepared $Ti_3C_2T_X$ membranes were superior to the state-of-the-art membranes. Moreover, MD simulations were further carried out to investigate the mechanism of selective gas diffusion in MXene membranes. Results showed that the MXene membrane structure significantly influenced gas diffusion behaviors and therefore, the gas separation performance [81]. In a recent study, W. Q. Jin reported the fabrication of 20 nm-thick MXene membranes with the vacuum-assisted method [82]. Prepared ultra-thin MXene membranes showed outstanding molecular sieving property towards separating H_2 from mixed H_2/CO_2 gas pair. Moreover, it was found that interlayer spacing of MXene membranes could be precisely controlled by pillaring MXene nanosheets with borate and PEI molecules, showing excellent CO_2 separation performance transcending the upper bound of state-of-the-art membranes.

2.6.2. MXene-based composite membrane and MMMs

Besides in pure form, H. T. Jung further prepared 90 nm thick $Ti_3C_2T_x$–GO composite membranes for water treatment and molecular separation [83]. GO nanosheets were mixed with $Ti_3C_2T_x$ to minimize

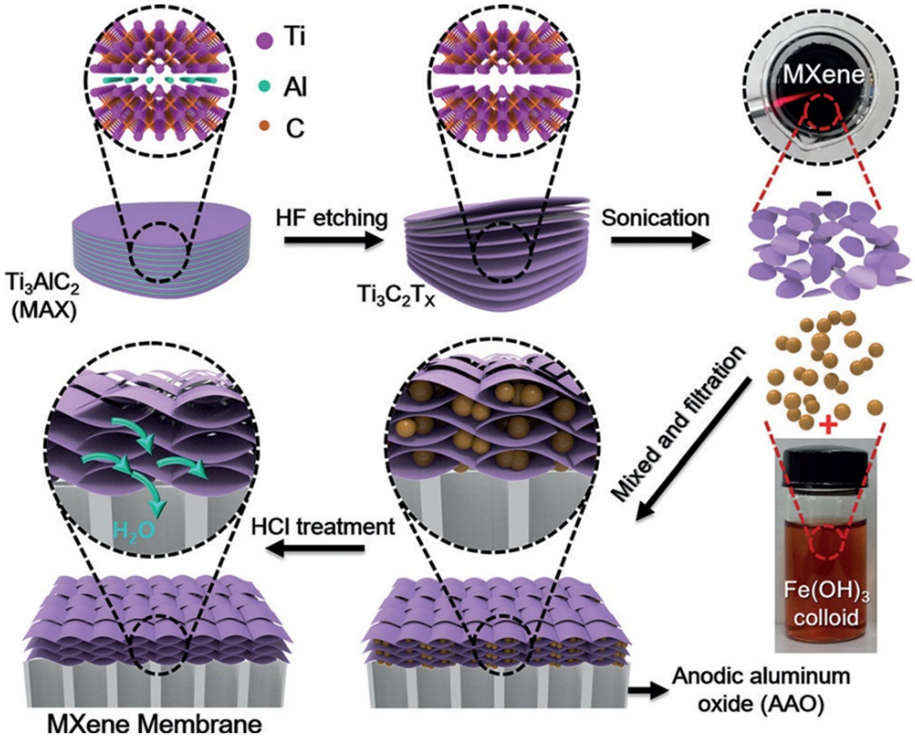

Fig. 15. Schematic illustration of the MXene membrane fabrication process.
(Reproduced with permission [78]. Copyright 2017, Wiley-VCH.)

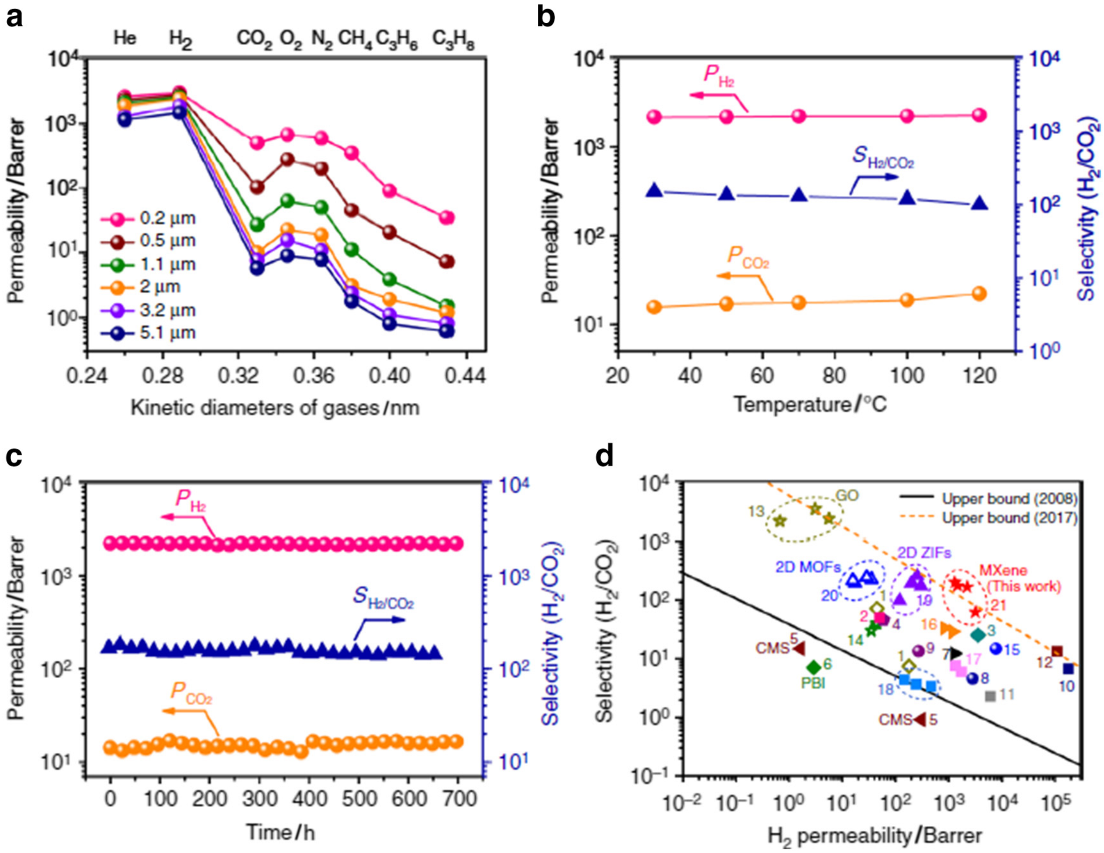

Fig. 16. a) Single-gas permeability through MXene membranes with different thicknesses; H_2/CO_2 separation performance of MXene membranes as a function of b) temperature and c) time; d) H_2/CO_2 separation performance of the MXene membranes compared with state-of-the-art gas separation membranes.
(Reproduced with permission [80]. Copyright 2018, Nature Publishing Group.)

the undesired penetration of guest molecules through nonselective channels (like inter-edge defects or voids). Prepared composite membranes effectively rejected dye molecules with hydrated radii above 0.5 nm as well as positively charged dye molecules. In the case of MXene-based MMMs, J. T. Wang further prepared $Ti_3C_2T_x$–PEI and $Ti_3C_2T_x$–PDMS MMMs for purification of alcohol-based mixtures [84]. Alcohol fluxes were found to be enhanced significantly due to a considerable promotion on the transfer of alcohol molecules along the nanosheet surface. Simultaneously, the rejection ratio was dramatically improved with MWCOs below 200 Da, owing to the blockage of solute transfer by nanosheets.

Post-modification represented an effective method for improving the separation performance of MXene membranes. Relying on abundant surface groups on $Ti_3C_2T_x$ sheets, diverse functional groups, including —NH_2, —COOR, —C_6H_6 and —$C_{12}H_{26}$, were grafted on their surface, respectively [85]. Interestingly, all functional groups grafted on $Ti_3C_2T_x$ sheets enhanced the flux for isopropanol, ethyl acetate, toluene and *n*-heptane, irrespective of hydrophilicity/hydrophobicity of the polymer matrix.

2.7. 2D g-C_3N_4 membrane

Recently great attention has been paid to 2D g-C_3N_4 materials composed of g-C_3N_4 sheets stacked together *via* weak van der Waals interactions [86]. Layered g-C_3N_4 sheets consists of tri-*s*-triazine units interconnected with tertiary amino groups forming regularly distributed triangular 0.311 nm-sized nanopores. It was predicted that these nanopores may allow preferential permeation of small-sized molecules (like H_2O, He and H_2) through g-C_3N_4-based membranes. In addition, unique physicochemical property, outstanding thermal and chemical stability as well as the low production cost have made g-C_3N_4 materials ideal candidates for membrane-based separation.

2.7.1. Pure g-C_3N_4 membrane

Relying on first-principle calculations, M. W. Zhao theoretically demonstrated that g-C_3N_4 membranes held great potential in He separation from other gas molecules [87]. The He/H_2 selectivity at R.T. was calculated to be ~10^7. Moreover, theoretically g-C_3N_4 membranes may also serve as competent quantum sieving membranes for $^3He/^4He$ separation with a selectivity of 18 at 49 K.

H. H. Wang fabricated AAO-supported 2D g-C_3N_4 membranes with artificial nanopores and self-supporting spacers by vacuum filtration (Fig. 17) [88]. Prepared 160 nm-thick g-C_3N_4 membranes showed a water flux of 290 $L\cdot m^{-2}\cdot h^{-1}\cdot MPa^{-1}$ with a rejection rate of 87% for 3 nm-sized molecules. Moreover, permeation experiments and molecular dynamic simulations further indicated the dominance of a nanofluidic phenomenon. In a follow-up study, polyacrylic acid (PAA) was introduced to regulate nanochannels formed between neighboring g-C_3N_4 nanosheets [89]. Prepared g-C_3N_4-PAA hybrid membranes possessed higher water flux without sacrificing much rejection rate. Nevertheless, noticeable fouling was observed upon the addition of PAA.

2.7.2. g-C_3N_4-based MMMs

Improving the dispersity of g-C_3N_4 in the polymer matrix represented an effective approach for enhancing the separation performance of g-C_3N_4-based MMMs. To achieve this purpose, Y. M. Li synthesized acidified g-C_3N_4 with smaller size and higher solubility [90]. Compared with pure polyamide (PA) membranes, acidified g-C_3N_4–PA MMMs exhibited a 79.3% increase in permeate flux while maintaining a quite high NaCl rejection ratio as well as an improved antifouling performance.

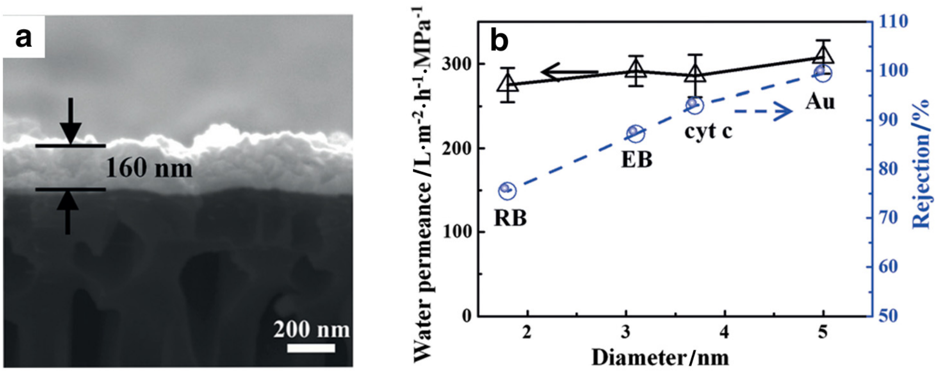

Fig. 17. a) A cross-sectional view of g-C_3N_4 membranes as a stack of nanosheets supported on porous AAO substrates and b) separation performance of g-C_3N_4 membranes as a function of the diameter of the largest cross-section of rejected molecules.
(Reproduced with permission [88]. Copyright 2017, Wiley-VCH.)

Z. Y. Jiang prepared g-C_3N_4–PIM MMMs by simple physical blending [91]. It was found that incorporation 2D g-C_3N_4 sheets in PIM-1 matrices influenced the packing of PIM-1 polymer chains and created additional diffusion pathways at the interface, resulting in an increment of permeability coefficients; moreover, periodic in-plane triangular nanopores of g-C_3N_4 sheets facilitated preferential permeation of H_2 so that H_2/CH_4 and H_2/N_2 selectivities were improved without any compromise in gas permeability. In the same manner, F. S. Pan further prepared g-C_3N_4–sodium alginate (SA) MMMs for pervaporation dehydration of water/ethanol mixtures [92]. Additional interfacial diffusion paths and regularly arranged in-plane nanopores jointly contributed to excellent water permeability and water/ethanol selectivity for g-C_3N_4–SA MMMs. In addition, prepared MMMs exhibited excellent long-term stability, owing to the strong interfacial forces. Y. J. Zhao further incorporated g-C_3N_4 nanosheets into a poly(vinyl alcohol) (PVA) matrix, showing improved water flux and separation factor for H_2O/ethanol mixtures as well as enhanced swelling resistance, mechanical stability and heat-resistance properties [93].

T. W. Xu further modified porous polyethersulfone (PES) substrates with r-GO/g-C_3N_4 for preparation of high performance thin film composite (TFC) polyamide forward osmosis (FO) membranes [94]. Results indicated that incorporation of r-GO/g-C_3N_4 resulted in ~20% increase of water flux, which could be attributed to the optimization of pore structure, enhanced wettability and the lower structure parameter.

X. Quan prepared g-C_3N_4/r-GO/CA composite photocatalytic membranes by assembling g-C_3N_4/r-GO photocatalysts on CA supports *via* vacuum filtration and N_2 pressing [95]. Owing to the high visible-light photocatalytic activity of g-C_3N_4 and photogenerated charge separation resulting from hetero-structure between g-C_3N_4 and r-GO, prepared composite membranes exhibited superior performance in water treatment (like Rhodamine B, COD_{Mn}, TOC, UV_{254} and bacteria removal) under visible light irradiation than membrane filtration alone.

2.8. Other emerging 2D separation membranes

Similar to graphite, h-BN also possesses a layered structure in which B and N atoms are bound by strong covalent bonds, whereas single h-BN nanosheets are held together by weak van der Waals interactions. Since h-BN is extremely stable under harsh conditions (such as acidic and basic solutions), h-BN-based separation membranes have become very attractive for organic solvent and water separation applications. Nevertheless, it has proven quite challenging to fabricate high quality h-BN separation membranes due to the poor water dispersibility and intrinsic hydrophobicity of h-BN nanosheets. To alleviate this problem, W. W. Lei developed amino-functionalized boron nitride (FBN) membranes by vacuum filtration of water-dispersible FBN flakes on porous Nylon substrates [96]. Prepared membranes showed not only excellent resistance to water and organic solution, but also considerable acidic, alkaline, and oxidative media stability. Moreover, prepared FBN-based membrane exhibited considerable separation performances in both aqueous and organic solvents due to the small size of FBN flakes and stable nanochannels between neighboring FBN flakes, showing promising perspectives in industrial separation and purification applications.

MT, which have the general formula $(Na,Ca)_{0.33}(Al,Mg)_2(Si_4O_{10})(OH)_2 \cdot nH_2O$, are representative of cationic clays composed of two tetrahedral sheets of silica sandwiching a central octahedral sheet of alumina. Compositional flexibility in both the negatively charged layers and charge-balancing cations gives rise to a functional diversity. The uniform and highly adjustable interlayer spacing of MT makes them ideal candidates for membrane-based separations. In a recent study, Z. Wang and M. D. Guiver prepared MT/PSf MMMs containing aligned MT interlayer galleries as high-speed CO_2 transport channels [97]. MT layers were bonded and aligned onto porous PSf substrates with the chain stretching orientation of polyvinylamine acid. Resulting MT/PSf membranes exhibited high CO_2 permeance and mixed-gas selectivity, making them potentially useful for CO_2 capture from flue gas or CO_2 removal from natural gas and syngas.

3. Conclusion and Perspective

To summarize, in the past decades a major breakthrough has been made in the field of 2D separation membranes, relying on the theoretic atomic-level thickness, diversified permeation paths and mechanical flexibility. Besides graphene and its derivatives (like GOs), other emerging 2D layered materials, like 2D zeolites, 2D MOFs, 2D COFs, LDHs, TMDCs, MXenes, g-C_3N_4, h-BN and MT, have shown unprecedented performances in microfiltration, nanofiltration, ultrafiltration, reverse osmosis, pervaporation and gas separation. Considering their structural and functional diversity, it is believed that 2D layered materials as building blocks will continue to contribute significantly to the performance enhancement of molecular sieve membranes and their widespread applications in industry.

Nevertheless, several critical issues are yet to be solved in further commercialization of 2D membranes.

1) Facile methods for bottom-up synthesis of 2D nanosheet building blocks. At present 2D nanosheets were obtained mainly through controlled exfoliation of their bulk layered counterparts. Nevertheless, it's still a big challenge to obtain highly monodispersed nanosheet building blocks with few in-plane defects and considerable productivity. In contrast, although still in its infancy, the bottom-up approach was considered very attractive and promising for bulk production of high quality 2D nanosheets as has been confirmed by recent studies [98–100].
2) Uniform deposition or distribution of nanosheet building blocks. As mentioned above, microstructures of 2D membranes exerted great

influence on their separation performances. For instance, uniform spatial arrangement of 2D nanosheet building blocks was considered advantageous for elimination of non-selective diffusion paths of guest molecules in the case of both 2D-material-based pure membranes and MMMs. It is therefore anticipated that an innovative process allowing regular deposition or distribution of monodispersed 2D nanosheets with controlled microstructures could be developed.

3) Creation of uniform in-plane nanopores on non-porous nanosheets. First-principle MD simulations have demonstrated the great potential of graphene, TMDC and MXene nanosheets in membrane-based separation (like gas separation and desalination) in case uniform in-plane nanopores with controlled shape, size, functionality and density were created. At present, diverse techniques like ion beam irradiation [101], oxygen plasma etching [102] and oxidative etching [103] have demonstrated their competence in drilling nanopores in non-porous nanosheets; nevertheless, these techniques are still far from mature. Therefore, reliable methods allowing precise microstructural manipulation of drilled in-plane nanopores in a large scale were urgently required.

References

[1] D.S. Sholl, R.P. Lively, Seven chemical separations to change the world, *Nature* 532 (2016) 435–437.

[2] H.B. Park, J. Kamcev, L.M. Robeson, M. Elimelech, B.D. Freeman, Maximizing the right stuff: The trade-off between membrane permeability and selectivity, *Science* 356 (2017) 1138–1148.

[3] K. Varoon, X.Y. Zhang, B. Elyassi, D.D. Brewer, M. Gettel, S. Kumar, J.A. Lee, S. Maheshwari, A. Mittal, C.Y. Sung, M. Cococcioni, L.F. Francis, A.V. McCormick, K.A. Mkhoyan, M. Tsapatsis, Dispersible exfoliated zeolite nanosheets and their application as a selective membrane, *Science* 334 (2011) 72–75.

[4] H. Li, Z.N. Song, X.J. Zhang, Y. Huang, S.G. Li, Y.T. Mao, H.J. Ploehn, Y. Bao, M. Yu, Ultrathin, molecular-sieving graphene oxide membranes for selective hydrogen separation, *Science* 342 (2013) 95–98.

[5] H.W. Kim, H.W. Yoon, S.-M. Yoon, B.M. Yoo, B.K. Ahn, Y.H. Cho, H.J. Shin, H. Yang, U. Paik, S. Kwon, J.-Y. Choi, H.B. Park, Selective gas transport through few-layered graphene and graphene oxide membranes, *Science* 342 (2013) 91–95.

[6] G.P. Liu, W.Q. Jin, N.P. Xu, Two-dimensional-material membranes: A new family of high-performance separation membranes, *Angew. Chem. Int. Ed.* 55 (2016) 13384–13397.

[7] J.Y. Zhu, J.W. Hou, A. Uliana, Y.T. Zhang, M.M. Tian, B. Van der Bruggen, The rapid emergence of two-dimensional nanomaterials for high-performance separation membranes, *J. Mater. Chem. A* 6 (2018) 3773–3792.

[8] A.K. Geim, Graphene: Status and prospects, *Science* 324 (2009) 1530–1534.

[9] S.P. Koenig, L.D. Wang, J. Pellegrino, J.S. Bunch, Selective molecular sieving through porous graphene, *Nat. Nanotechnol.* 7 (2012) 728–732.

[10] R.R. Nair, H.A. Wu, P.N. Jayaram, I.V. Grigorieva, A.K. Geim, Unimpeded permeation of water through helium-leak-tight graphene-based membranes, *Science* 335 (2012) 442–444.

[11] G.P. Liu, W.Q. Jin, N.P. Xu, Graphene-based membranes, *Chem. Soc. Rev.* (15) (2015) 5016–5030.

[12] N. Song, X.L. Gao, Z. Ma, X.J. Wang, Y. Wei, C.J. Gao, A review of graphene-based separation membranes: Materials, characteristics, preparation and applications, *Desalination* 437 (2018) 59–72.

[13] W. Kim, S. Nair, Membranes from nanoporous 1D and 2D materials: A review of opportunities, developments, and challenges, *Chem. Eng. Sci.* 104 (2013) 908–924.

[14] X. Zhu, C.C. Tian, C.L. Do-Thanh, S. Dai, Two-dimensional materials as prospective scaffolds for mixed-matrix membrane-based CO_2 separation, *ChemSusChem* 10 (2017) 3304–3316.

[15] Z.K. Zheng, R. Gruenker, X.L. Feng, Synthetic two-dimensional materials: A new paradigm of membranes for ultimate separation, *Adv. Mater.* 28 (2016) 6529–6545.

[16] A. Gugliuzza, A. Politano, E. Drioli, The advent of graphene and other two-dimensional materials in membrane science and technology, *Curr. Opin. Chem. Eng.* 16 (2017) 78–85.

[17] Y.L. Ying, Y.F. Yang, W. Ying, X.S. Peng, Two-dimensional materials for novel liquid separation membranes, *Nanotechnology* 27 (2016) 332001.

[18] Y.D. Zhao, Y.Z. Xie, Z.K. Liu, X.S. Wang, Y. Chai, F. Yan, Two-dimensional material membranes: An emerging platform for controllable mass transport applications, *Small* 10 (2014) 4521–4542.

[19] J. Choi, Z.P. Lai, S. Ghosh, D.E. Beving, Y.S. Yan, M. Tsapatsis, Layer-by-layer deposition of barrier and permselective c-oriented-MCM-22/silica composite membranes, *Ind. Eng. Chem. Res.* 46 (2007) 7096–7106.

[20] J. Choi, M. Tsapatsis, MCM-22/silica selective flake nanocomposite membranes for hydrogen separations, *J. Am. Chem. Soc.* 132 (2010) 448–449.

[21] M. Choi, K. Na, J. Kim, Y. Sakamoto, O. Terasaki, R. Ryoo, Stable single-unit-cell nanosheets of zeolite MFI as active and long-lived catalysts, *Nature* 461 (2009) 246–249.

[22] K. Na, M. Choi, W. Park, Y. Sakamoto, O. Terasaki, R. Ryoo, Pillared MFI zeolite nanosheets of a single-unit-cell thickness, *J. Am. Chem. Soc.* 132 (2010) 4169–4177.

[23] H. Zhang, Q. Xiao, X.H. Guo, N.J. Li, P. Kumar, N. Rangnekar, M.Y. Jeon, S. Al-Thabaiti, K. Narasimharao, S.N. Basahel, B. Topuz, F.J. Onorato, C.W. Macosko, K.A. Mkhoyan, M. Tsapatsis, Open-pore two-dimensional MFI zeolite nanosheets for the fabrication of hydrocarbon-isomer-selective membranes on porous polymer supports, *Angew. Chem. Int. Ed.* 55 (2016) 7184–7187.

[24] D. Kim, M.Y. Jeon, B.L. Stottrup, M. Tsapatsis, para-Xylene ultra-selective zeolite MFI membranes fabricated from nanosheet monolayers at the air–water interface, *Angew. Chem. Int. Ed.* 57 (2018) 480–485.

[25] K.V. Agrawal, B. TopuZ, T.C.T. Pham, T.H. Nguyen, N. Sauer, N. Rangnekar, H. Zhang, K. Narasimharao, S.N. Basahel, L.F. Francis, C.W. Macosko, S. Al-Thabaiti, M. Tsapatsis, K.B. Yoon, Oriented MFI membranes by gel-less secondary growth of sub-100 nm MFI-nanosheet seed layers, *Adv. Mater.* 27 (2015) 3243–3249.

[26] M.Y. Jeon, D. Kim, P. Kumar, P.S. Lee, N. Rangnekar, P. Bai, M. Shete, B. Elyassi, H.S. Lee, K. Narasimharao, S.N. Basahel, S. Al-Thabaiti, W.Q. Xu, H.J. Cho, E.O. Fetisov, R. Thyagarajan, R.F. DeJaco, W. Fan, K.A. Mkhoyan, J.I. Siepmann, M. Tsapatsis, Ultra-selective high-flux membranes from directly synthesized zeolite nanosheets, *Nature* 543 (2017) 690–694.

[27] S. Choi, J. Coronas, E. Jordan, W. Oh, S. Nair, F. Onorato, D.F. Shantz, M. Tsapatsis, Layered silicates by swelling of AMH-3 and nanocomposite membranes, *Angew. Chem. Int. Ed.* 47 (2008) 552–555.

[28] W. Kim, J.S. Lee, D.G. Bucknall, W.J. Koros, S. Nair, Nanoporous layered silicate AMH-3/cellulose acetate nanocomposite membranes for gas separations, *J. Membr. Sci.* 441 (2013) 129–136.

[29] A. Galve, D. Sieffert, E. Vispe, C. Tellez, J. Coronas, C. Staudt, Copolyimide mixed matrix membranes with oriented microporous titanosilicate JDF-L1 sheet particles, *J. Membr. Sci.* 370 (2011) 131–140.

[30] S. Castarlenas, P. Gorgojo, C. Casado-Coterillo, S. Masheshwari, M. Tsapatsis, C. Tellez, J. Coronas, Melt compounding of swollen titanosilicate JDF-L1 with polysulfone to obtain mixed matrix membranes for H_2/CH_4 separation, *Ind. Eng. Chem. Res.* 52 (2013) 1901–1907.

[31] A. Galve, D. Sieffert, C. Staudt, M. Ferrando, C. Guell, C. Tellez, J. Coronas, Combination of ordered mesoporous silica MCM-41 and layered titanosilicate JDF-L1 fillers for 6FDA-based copolyimide mixed matrix membranes, *J. Membr. Sci.* 431 (2012) 163–170.

[32] M.A. Camblor, A. Corma, M.J. Diaz-Cabanas, C. Baerlocher, Synthesis and structural characterization of MWW type zeolite ITQ-1, the pure silica analog of MCM-22 and SSZ-25, *J. Phys. Chem. B* 102 (1998) 44–51.

[33] M.H. Zhu, Y.S. Liu, Y.K. Yao, J.M. Jiang, F. Zhang, Z. Yang, Z.H. Lu, I. Kumakiri, X.S. Chen, H. Kita, Preparation and catalytic performance of Ti-MWW zeolite membrane for phenol hydroxylation, *Microporous Mesoporous Mater.* 268 (2018) 84–87.

[34] Y. Peng, Y.S. Li, Y.J. Ban, H. Jin, W.M. Jiao, X.L. Liu, W.S. Yang, Metal–organic framework nanosheets as building blocks for molecular sieving membranes, *Science* 346 (2014) 1356–1359.

[35] Y. Peng, Y.S. Li, Y.J. Ban, W.S. Yang, Two-dimensional metal–organic framework nanosheets for membrane-based gas separation, *Angew. Chem. Int. Ed.* 56 (2017) 9757–9761.

[36] X.R. Wang, C.L. Chi, K. Zhang, Y.H. Qian, K.M. Gupta, Z.X. Kang, J.W. Jiang, D. Zhao, Reversed thermo-switchable molecular sieving membranes composed of two-dimensional metal–organic nanosheets for gas separation, *Nat. Commun.* 8 (2017) 14460.

[37] Z.X. Zhong, J.F. Yao, R.Z. Chen, Z.X. Low, M. He, J.Z. Liu, H.T. Wang, Oriented two-dimensional zeolitic imidazolate framework-L membranes and their gas permeation properties, *J. Mater. Chem. A* 3 (2015) 15715–15722.

[38] W.B. Li, P.C. Su, Z.J. Li, Z.H. Xu, F. Wang, H.S. Ou, J.H. Zhang, G.L. Zhang, E. Zeng, Ultrathin metal–organic framework membrane production by gel–vapour deposition, *Nat. Commun.* 8 (2017) 406.

[39] H.X. Ang, L. Hong, Polycationic polymer-regulated assembling of 2D MOF nanosheets for high-performance nanofiltration, *ACS Appl. Mater. Interfaces* 9 (2017) 28079–28088.

[40] T. Rodenas, I. Luz, G. Prieto, B. Seoane, H. Miro, A. Corma, F. Kapteijn, F.X. Llabres i Xamena, J. Gascon, Metal–organic framework nanosheets in polymer composite materials for gas separation, *Nat. Mater.* 14 (2015) 48–55.

[41] Z.X. Kang, Y.W. Peng, Z.G. Hu, Y.H. Qian, C.L. Chi, L.Y. Yeo, L. Tee, D. Zhao, Mixed matrix membranes composed of two-dimensional metal–organic framework nanosheets for pre-combustion CO_2 capture: A relationship study of filler morphology versus membrane performance, *J. Mater. Chem. A* 3 (2015) 20801–20810.

[42] Y.D. Cheng, X.R. Wang, C.K. Jia, Y.X. Wang, L.Z. Zhai, Q. Wang, D. Zhao, Ultrathin mixed matrix membranes containing two-dimensional metal–organic framework nanosheets for efficient CO_2/CH_4 separation, *J. Membr. Sci.* 539 (2017) 213–223.

[43] G.H. Liu, Z.Y. Jiang, K.T. Cao, S. Nair, X.X. Cheng, J. Zhao, H. Gomaa, H. Wu, F.S. Pan, Pervaporation performance comparison of hybrid membranes filled with two-dimensional ZIF-L nanosheets and zero-dimensional ZIF-8 nanoparticles, *J. Membr. Sci.* 523 (2017) 185–196.

[44] Y. Lo, D.Y. Kang, Pseudopolymorphic seeding for the rational synthesis of hybrid membranes with a zeolitic imidazolate framework for enhanced molecular separation performance, *J. Mater. Chem. A* 4 (2016) 4172–4179.

[45] Y. Wang, J.P. Li, Q.Y. Yang, C.L. Zhong, Two-dimensional covalent triazine framework membrane for helium separation and hydrogen purification, *ACS Appl. Mater. Interfaces* 8 (2016) 8694–8701.

[46] M.M. Tong, Q.Y. Yang, Q.T. Ma, D.H. Liu, C.L. Zhong, Few-layered ultrathin covalent organic framework membranes for gas separation: A computational study, *J. Mater. Chem. A* 4 (2016) 124–131.

[47] G. Li, K. Zhang, T. Tsuru, Two-dimensional covalent organic framework (COF) membranes fabricated via the assembly of exfoliated COF nanosheets, *ACS Appl. Mater. Interfaces* 9 (2017) 8433–8436.

[48] Z.X. Kang, Y.W. Peng, Y.H. Qian, D.Q. Yuan, M.A. Addicoat, T. Heine, Z.G. Hu, L. Tee, Z.G. Guo, D. Zhao, Mixed matrix membranes (MMMs) comprising exfoliated 2D covalent organic frameworks (COFs) for efficient CO_2 separation, *Chem. Mater.* 28 (2016) 1277–1285.

[49] Y.P. Ying, D.H. Liu, J. Ma, M.M. Tong, W.X. Zhang, H.L. Huang, Q.Y. Yang, C.L. Zhong, A GO-assisted method for the preparation of ultrathin covalent organic framework membranes for gas separation, *J. Mater. Chem. A* 4 (2016) 13444–13449.

[50] H.W. Fan, J.H. Gu, H. Meng, A. Knebel, J. Caro, High-flux membranes based on the covalent organic framework COF-LZU1 for selective dye separation by nanofiltration, *Angew. Chem. Int. Ed.* 57 (2018) 4083–4087.

[51] T.W. Kim, M. Sahimi, T.T. Tsotsis, The preparation and characterization of hydrotalcite thin films, *Ind. Eng. Chem. Res.* 48 (2009) 5794–5801.

[52] T.W. Kim, M. Sahimi, T.T. Tsotsis, The preparation and characterization of hydrotalcite micromembranes, *Chem. Eng. Sci.* 64 (2009) 1585–1590.

[53] T.W. Kim, M. Sahimi, T.T. Tsotsis, Preparation of hydrotalcite thin films using an electrophoretic technique, *Ind. Eng. Chem. Res.* 47 (2008) 9127–9132.

[54] Y. Liu, N.Y. Wang, Z.W. Cao, J. Caro, Molecular sieving through interlayer galleries, *J. Mater. Chem. A* 2 (2014) 1235–1238.

[55] Y. Liu, N.Y. Wang, J. Caro, In situ formation of LDH membranes of different microstructures with molecular sieve gas selectivity, *J. Mater. Chem. A* 2 (2014) 5716–5723.

[56] Y. Liu, J.H. Pan, N.Y. Wang, F. Steinbach, X.L. Liu, J. Caro, Remarkably enhanced gas separation by partial self-conversion of a laminated membrane to metal–organic frameworks, *Angew. Chem. Int. Ed.* 54 (2015) 3028–3032.

[57] J.Y. Liao, Z. Wang, C.Y. Gao, S.C. Li, Z.H. Qiao, M. Wang, S. Zhao, X.M. Xie, J.X. Wang, S.C. Wang, Fabrication of high-performance facilitated transport membranes for CO_2 separation, *Chem. Sci.* 5 (2014) 2843–2849.

[58] Y. Liu, N.Y. Wang, L. Diestel, F. Steinbach, J. Caro, MOF membrane synthesis in the confined space of a vertically aligned LDH network, *Chem. Commun.* 50 (2014) 4225–4227.

[59] Y. Liu, N.Y. Wang, J.H. Pan, F. Steinbach, J. Caro, *In situ* synthesis of MOF membranes on ZnAl–CO_3 LDH buffer layer-modified substrates, *J. Am. Chem. Soc.* 136 (2014) 14353–14356.

[60] Y. Liu, Y. Peng, N.Y. Wang, Y.S. Li, J.H. Pan, W.S. Yang, J. Caro, Significantly enhanced separation using ZIF-8 membranes by partial conversion of calcined layered double hydroxide precursors, *ChemSusChem* 8 (2015) 3582–3586.

[61] S. Manzeli, D. Ovchinnikov, D. Pasquier, O.V. Yazyev, A. Kis, 2D transition metal dichalcogenides, *Nat. Rev. Mater.* 2 (2017) 17033.

[62] J. Azamat, A. Khataee, Improving the performance of heavy metal separation from water using MoS_2 membrane: Molecular dynamics simulation, *Comput. Mater. Sci.* 137 (2017) 201–207.

[63] W.F. Li, Y.M. Yang, J.K. Weber, G. Zhang, R.H. Zhou, Tunable, strain-controlled nanoporous MoS_2 filter for water desalination, *ACS Nano* 10 (2016) 1829–1835.

[64] Y.D. Zhang, Z.S. Meng, Q. Shi, H.Q. Gao, Y.Z. Liu, Y.H. Wang, D.W. Rao, K.M. Deng, R.F. Lu, Nanoporous MoS_2 monolayer as a promising membrane for purifying hydrogen and enriching methane, *J. Phys. Condens. Matter* 29 (2017) 375201.

[65] L.W. Sun, H.B. Huang, X.S. Peng, Laminar MoS_2 membranes for molecular separation, *Chem. Commun.* 49 (2013) 10718–10720.

[66] D. Wang, Z.G. Wang, L. Wang, L. Hu, J. Jin, Ultrathin membranes of single-layered MoS_2 nanosheets for high-performance hydrogen separation, *Nanoscale* 7 (2015) 17649–17652.

[67] A. Achari, S. Sahana, M. Eswaramoorthy, High performance MoS_2 membranes: Effects of thermally driven phase transition on CO_2 separation efficiency, *Energy Environ. Sci.* 9 (2016) 1224–1228.

[68] M.M. Deng, K. Kwac, M. Li, Y. Jung, H.G. Park, Stability, molecular sieving and ion diffusion selectivity of a lamellar membrane from two-dimensional molybdenum disulfide, *Nano Lett.* 17 (2017) 2342–2348.

[69] Z.Y. Wang, B.X. Mi, Environmental applications of 2D molybdenum disulfide (MoS_2) nanosheets, *Environ. Sci. Technol.* 51 (2017) 8229–8244.

[70] W. Hirunpinyopas, E. Prestat, S.D. Worrall, S.J. Haigh, R.A.W. Dryfe, M.A. Bissett, Desalination and nanofiltration through functionalized laminar MoS_2 membranes, *ACS Nano* 11 (2017) 11082–11090.

[71] D.K. Chen, W. Ying, Y. Guo, Y.L. Ying, X.S. Peng, Enhanced gas separation through nanoconfined ionic liquid in laminated MoS_2 membrane, *ACS Appl. Mater. Interfaces* 9 (2017) 44251–44257.

[72] Y.J. Shen, H.X. Wang, X. Zhang, Y.T. Zhang, MoS_2 nanosheets functionalized composite mixed matrix membrane for enhanced CO_2 capture via surface drop-coating method, *ACS Appl. Mater. Interfaces* 8 (2016) 23371–23378.

[73] F.S. Pan, H. Ding, W.D. Li, Y.M. Song, H. Yang, H. Wu, Z.Y. Jiang, B.Y. Wang, X.Z. Cao, Constructing facilitated transport pathway in hybrid membranes by incorporating MoS_2 nanosheets, *J. Membr. Sci.* 545 (2018) 29–37.

[74] L.W. Sun, Y.L. Ying, H.B. Huang, Z.G. Song, Y.Y. Mao, Z.P. Xu, X.S. Peng, Ultrafast molecular separation through layered WS_2 nanosheet membranes, *ACS Nano* 8 (2014) 6304–6311.

[75] J.Y. Lin, R.X. Zhang, W.Y. Ye, N. Jullok, A. Sotto, B. Van der Bruggen, Nano-WS_2 embedded PES membrane with improved fouling and permselectivity, *J. Colloid Interface Sci.* 396 (2013) 120–128.

[76] M. Naguib, M. Kurtoglu, V. Presser, J. Lu, J. Niu, M. Heon, L. Hultman, Y. Gogotsi, M.W. Barsoum, Two-dimensional nanocrystals produced by exfoliation of Ti_3AlC_2, *Adv. Mater.* 23 (2011) 4248–4253.

[77] C.E. Ren, K.B. Hatzell, M. Alhabeb, Z. Ling, K.A. Mahmoud, Y. Gogotsi, Charge- and size-selective ion sieving through $Ti_3C_2T_x$ MXene membranes, *J. Phys. Chem. Lett.* 6 (2015) 4026–4031.

[78] L. Ding, Y.Y. Wei, Y.J. Wang, H.B. Chen, J. Caro, H.H. Wang, A two-dimensional lamellar membrane: MXene nanosheet stacks, *Angew. Chem. Int. Ed.* 56 (2017) 1825–1829.

[79] G.Z. Liu, J. Shen, Q. Liu, G.P. Liu, J. Xiong, J. Yang, W.Q. Jin, Ultra-thin two-dimensional MXene membrane for pervaporation desalination, *J. Membr. Sci.* 548 (2018) 548–558.

[80] L. Ding, Y.Y. Wei, L.B. Li, T. Zhang, H.H. Wang, J. Xue, L.X. Ding, S.Q. Wang, J. Caro, Y. Gogotsi, MXene molecular sieving membranes for highly efficient gas separation, *Nat. Commun.* 9 (2018) 155.

[81] L.B. Li, T. Zhang, Y.F. Duan, Y.Y. Wei, C.J. Dong, L. Ding, Z.W. Qiao, H.H. Wang, Selective gas diffusion in two-dimensional MXene lamellar membranes: Insights from molecular dynamics simulations, *J. Mater. Chem. A* 6 (2018) 11734–11742.

[82] J. Shen, G.Z. Liu, Y.F. Ji, Q. Liu, L. Cheng, K.C. Guan, M.C. Zhang, G.P. Liu, J. Xiong, J. Yang, W.Q. Jin, 2D MXene nanofilms with tunable gas transport channels, *Adv. Funct. Mater.* (2018) 1801511.

[83] K.M. Kang, D.W. Kim, C.E. Ren, K.M. Cho, S.J. Kim, J.H. Choi, Y.T. Nam, Y. Gogotsi, H.T. Jung, Selective molecular separation on $Ti_3C_2T_x$–graphene oxide membranes during pressure-driven filtration: Comparison with graphene oxide and MXenes, *ACS Appl. Mater. Interfaces* 9 (2017) 44687–44694.

[84] X.L. Wu, L. Hao, J.K. Zhang, X. Zhang, J.T. Wang, J.D. Liu, Polymer–$Ti_3C_2T_x$ composite membranes to overcome the trade-off in solvent resistant nanofiltration for alcohol-based system, *J. Membr. Sci.* 515 (2016) 175–188.

[85] L. Hao, H.Q. Zhang, X.L. Wu, J.K. Zhang, J.T. Wang, Y.F. Li, Novel thin-film nanocomposite membranes filled with multi-functional Ti_3C_2Tx nanosheets for task-specific solvent transport, *Compos. A: Appl. Sci. Manuf.* 100 (2017) 139–149.

[86] A. Thomas, A. Fischer, F. Goettmann, M. Antonietti, J.O. Mgller, R. Schlçgl, J.M. Carlsson, Graphitic carbon nitride materials: Variation of structure and morphology and their use as metal-free catalysts, *J. Mater. Chem.* 18 (2008) 4893–4908.

[87] F. Li, Y.Y. Qu, M.W. Zhao, Efficient helium separation of graphitic carbon nitride membrane, *Carbon* 95 (2015) 51–57.

[88] Y.J. Wang, L.B. Li, Y.Y. Wei, J. Xue, H. Chen, L. Ding, J. Caro, H.H. Wang, Water transport with ultralow friction through partially exfoliated g-C_3N_4 nanosheet membranes with self-supporting spacers, *Angew. Chem. Int. Ed.* 56 (2017) 8974–8980.

[89] Y.J. Wang, L.F. Liu, J. Xue, J.M. Hou, L. Ding, H.H. Wang, Enhanced water flux through graphitic carbon nanosheets membrane by incorporating polyacrylic acid, *AIChE J.* 64 (2018) 2181–2188.

[90] X. Gao, Y.M. Li, X.L. Yang, Y.N. Shang, Y. Wang, B.Y. Gao, Z.N. Wang, Highly permeable and antifouling reverse osmosis membranes with acidified graphitic carbon nitride nanosheets as nanofillers, *J. Mater. Chem. A* 5 (2017) 19875–19883.

[91] Z.Z. Tian, S.F. Wang, Y.T. Wang, X.R. Ma, K.T. Cao, D.D. Peng, X.Y. Wu, H. Wu, Z.Y. Jiang, Enhanced gas separation performance of mixed matrix membranes from graphitic carbon nitride nanosheets and polymers of intrinsic microporosity, *J. Membr. Sci.* 514 (2016) 15–24.

[92] K.T. Cao, Z.Y. Jiang, X.S. Zhang, Y.M. Zhang, J. Zhao, R.S. Xing, S. Yang, C.Y. Gao, F.S. Pan, Highly water-selective hybrid membrane by incorporating g-C_3N_4 nanosheets into polymer matrix, *J. Membr. Sci.* 490 (2015) 72–83.

[93] J. Wang, M.S. Li, S.Y. Zhou, A.L. Xue, Y. Zhang, Y.J. Zhao, J. Zhong, Q. Zhang, Graphitic carbon nitride nanosheets embedded in poly(vinyl alcohol) nanocomposite membranes for ethanol dehydration via pervaporation, *Sep. Purif. Technol.* 188 (2017) 24–37.

[94] Y.Q. Wang, R.W. Ou, H.T. Wang, T.W. Xu, Graphene oxide modified graphitic carbon nitride as a modifier for thin film composite forward osmosis membrane, *J. Membr. Sci.* 475 (2015) 281–289.

[95] H.X. Zhao, S. Chen, X. Quan, H.T. Yu, H.M. Zhao, Integration of microfiltration and visible-light-driven photocatalysis on g-C_3N_4 nanosheet/reduced graphene oxide membrane for enhanced water treatment, *Appl. Catal. B Environ.* 194 (2016) 134–140.

[96] C. Chen, J.M. Wang, D. Liu, C. Yang, Y.C. Liu, R.S. Ruoff, W.W. Lei, Functionalized boron nitride membranes with ultrafast solvent transport performance for molecular separation, *Nat. Commun.* 9 (2018) 1902.

[97] Z.H. Qiao, S. Zhao, J.X. Wang, S.C. Wang, Z. Wang, M.D. Guiver, A highly permeable aligned montmorillonite mixed-matrix membrane for CO_2 separation, *Angew. Chem. Int. Ed.* 55 (2016) 9321–9325.

[98] M.T. Zhao, Y.X. Wang, Q.L. Ma, Y. Huang, X. Zhang, J.F. Ping, Z.C. Zhang, Q.P. Lu, Y.F. Yu, H. Xu, Y.L. Zhao, H. Zhang, Ultrathin 2D metal–organic framework nanosheets, *Adv. Mater.* 27 (2015) 7372–7378.

[99] R. Makiura, O. Konovalov, Bottom-up assembly of ultrathin sub-micron size metal–organic framework sheets, *Dalton Trans.* 42 (2013) 15931–15936.

[100] J.F. Yu, B.R. Martin, A. Clearfield, Z.P. Luo, L.Y. Sun, One-step direct synthesis of layered double hydroxide single-layer nanosheets, *Nanoscale* 7 (2015) 9448–9451.

[101] S.P. Surwade, S.N. Smirnov, I.V. Vlassiouk, R.R. Unocic, G.M. Veith, S. Dai, S.M. Mahurin, Water desalination using nanoporous single-layer graphene, *Nat. Nanotechnol.* 10 (2015) 459–464.

[102] H. Li, L. Daukiya, S. Haldar, A. Lindblad, B. Sanyal, O. Eriksson, D. Aubel, S. Hajjar-Garreau, L. Simon, K. Leifer, Site-selective local fluorination of graphene induced by focused ion beam irradiation, *Sci. Rep.* 6 (2016) 19719.

[103] X.L. Lu, R.G. Wang, L.F. Hao, F. Yang, W.C. Jiao, P. Peng, F. Yuan, W.B. Liu, Oxidative etching of MoS_2/WS_2 nanosheets to their QDs by facile UV irradiation, *Phys. Chem. Chem. Phys.* 18 (2016) 31211–31216.